

AD-A045 670

PRATT AND WHITNEY AIRCRAFT GROUP WEST PALM BEACH FLA --ETC F/G 21/5
RELIABILITY PREDICTION FOR COMBUSTORS AND TURBINES. VOLUME I.(U)
JUN 77 B C SCHLEIN

F33615-75-C-2057

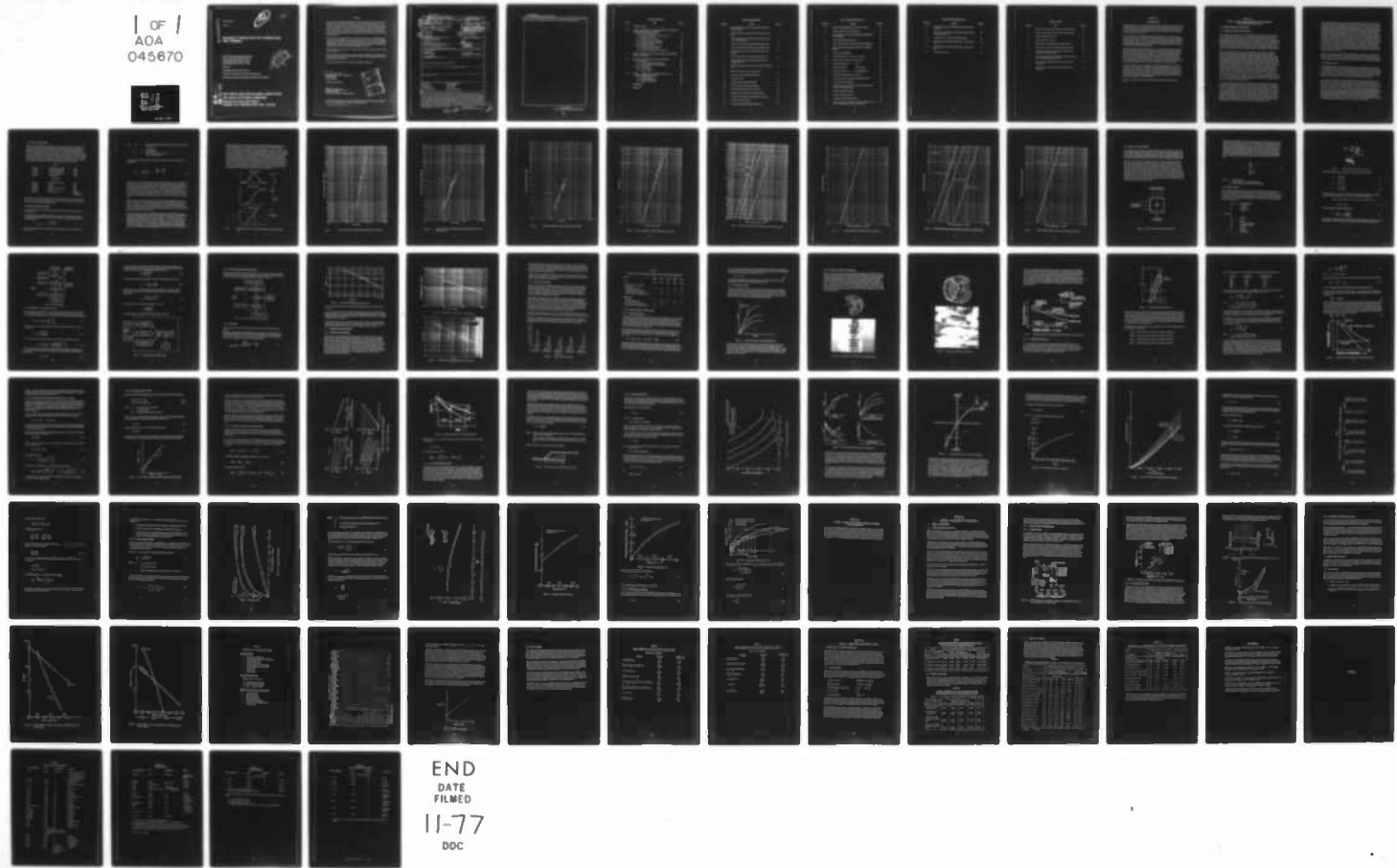
UNCLASSIFIED

FR-8187-VOL-1

AFAPL-TR-77-8-VOL-1

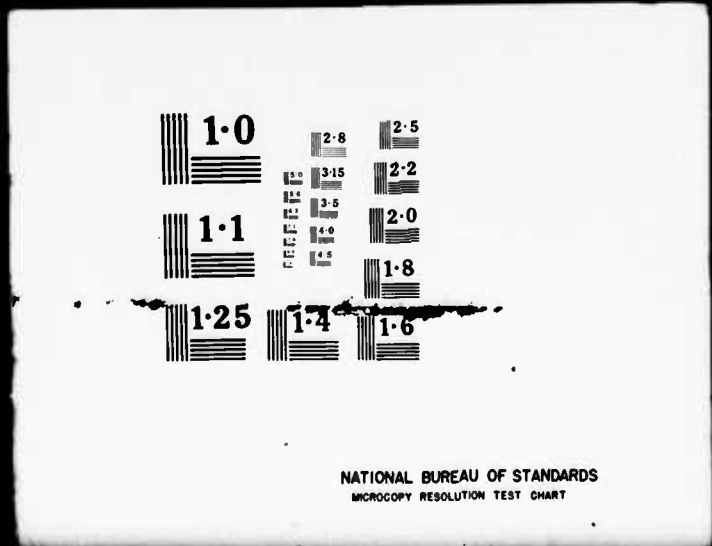
NL

1 OF 1
AOA
045670



END
DATE
FILED
11-77
DDC

| OF |
ADA
045670



AD A 045670

AFAPL-TR-77-8

Volume I

12

D

RELIABILITY PREDICTION FOR COMBUSTORS AND TURBINES

UNITED TECHNOLOGIES CORPORATION
PRATT & WHITNEY AIRCRAFT GROUP
GOVERNMENT PRODUCTS DIVISION
WEST PALM BEACH, FLORIDA 44402

JUNE 1977

TECHNICAL REPORT AFAPL-TR-77-8

Final Report for Period 25 June 1975 - 30 November 1976

APPROVED FOR PUBLIC RELEASE: DISTRIBUTION UNLIMITED



AD No. _____
DDC FILE COPY

AIR FORCE AERO PROPULSION LABORATORY
AIR FORCE SYSTEMS COMMAND
UNITED STATES AIR FORCE
WRIGHT-PATTERSON AFB, OHIO 45433

NOTICE

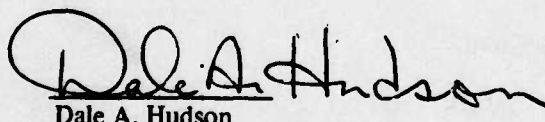
When Government drawings, specifications or other data are used for any purpose other than in connection with a definitely related Government procurement operation, the United States Government thereby incurs no responsibility nor any obligation whatsoever; and the fact that the government may have formulated, furnished, or in any way supplied the said drawings, specifications, or other data, is not to be regarded by implication or otherwise as in any manner licensing the holder or any other person or corporation, or conveying any rights or permission to manufacture, use, or sell any patented invention that may in any way be related thereto.

This final report was submitted by Pratt & Whitney Aircraft Group, Government Products Division, United Technologies Corporation, under Contract F33615-75-C-2057. The effort was sponsored by the Air Force Aero Propulsion Laboratory, Air Force Systems Command, Wright-Patterson AFB, Ohio with Dale Hudson/TBC as Project Engineer. Barry Schlein of Pratt & Whitney Aircraft was technically responsible for the work.

Technical assistance provided by W. H. Vogel and M. T. Loferski was essential to the completion of the project.

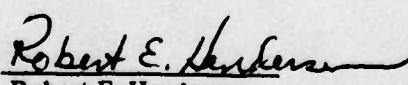
This report has been reviewed by the Information Office (ASD/OIP) and is releasable to the National Technical Information Service (NTIS). At NTIS, it will be available to the general public, including foreign nations.

This technical report has been reviewed and is approved for publication.



Dale A. Hudson
Project Engineer

FOR THE COMMANDER



Robert E. Henderson
Technical Area Manager, Combustion Group



Copies of this report should not be returned unless return is required by security considerations, contractual obligations, or notice on a specific document.

UNCLASSIFIED

SECURITY CLASSIFICATION OF THIS PAGE (When Data Entered)

(9) REPORT DOCUMENTATION PAGE		READ INSTRUCTIONS BEFORE COMPLETING FORM	
1. REPORT NUMBER AFAPL TR-77-8-Vol-1	2. GOVT ACCESSION NO.	3. RECIPIENT CATALOG NUMBER	
4. TITLE (and Subtitle) Reliability Predictions for Combustors and Turbines. Volume I.		5. TYPE OF REPORT & PERIOD COVERED Final <i>rept.</i> 15 June 1975 - 30 November 1976	
7. AUTHOR(s) B. C. Schlein		6. PERFORMING ORGANIZATION NUMBER (14) FR-8187-Vol-1	
9. PERFORMING ORGANIZATION NAME AND ADDRESS Pratt & Whitney Aircraft Group Government Products Division P. O. Box 2691 West Palm Beach, Florida 33402		10. PROGRAM ELEMENT, PROJECT, TASK AREA & WORK UNIT NUMBERS (15) F33615-75-C-2057-new	
11. CONTROLLING OFFICE NAME AND ADDRESS Air Force Aero Propulsion Laboratory /TBC Air Force Systems Command U. S. Air Force, Wright-Patterson AFB, Ohio 45433		12. REPORT DATE (11) June 1977	
14. MONITORING AGENCY NAME & ADDRESS(if different from Controlling Office) (12) 860 P.		13. NUMBER OF PAGES 86	
16. DISTRIBUTION STATEMENT (of this Report)		15. SECURITY CLASS. (of this report) UNCLASSIFIED	
		15a. DECLASSIFICATION/DOWNGRADING SCHEDULE	
17. DISTRIBUTION STATEMENT (of the abstract entered in Block 20, if different from Report)			
18. SUPPLEMENTARY NOTES			
19. KEY WORDS (Continue on reverse side if necessary and identify by block number) Reliability Turbine Durability Mission Analysis Failure Models Life Prediction Creep - LCF Combustor Durability Louver Lip Buckling			
20. ABSTRACT (Continue on reverse side if necessary and identify by block number) Creep - low cycle fatigue and louver lip collapse have been established as primary gas turbine combustion chamber failure modes by observation of field service and in-house endurance test hardware. Analytical models for these two failure modes have been developed and incorporated into a mission analysis program. The mission analysis program previously in use at P&WA with turbine airfoil failure models relates component environment (temperature, pressure and flow) to the aircraft engine and flight characteristics and thereby provides the forcing functions for the turbine and combustor failure models. The combined mission analysis - failure model program was used to predict compo-			

DD FORM 1473 EDITION OF 1 NOV 54 IS OBSOLETE

UNCLASSIFIED

SECURITY CLASSIFICATION OF THIS PAGE (When Data Entered)

SECURIT
392 887

UNCLASSIFIED

SECURITY CLASSIFICATION OF THIS PAGE(When Data Entered)

ment lives for transport and fighter/attack aircraft over representative missions. The sensitivity of the prediction system was established by perturbations to the mission and input parameters.

UNCLASSIFIED

SECURITY CLASSIFICATION OF THIS PAGE(When Data Entered)

N

TABLE OF CONTENTS

Section	Title	Page No.
1.0	INTRODUCTION	1
2.0	PHASE I - IDENTIFICATION AND MODELING OF COMBUSTOR AND TURBINE AIRFOIL FAILURES	2
2.1	Turbine Airfoil Failure Modes	2
2.1.1	Turbine Airfoil Failure Mechanism Review	2
2.1.2	Definition of Failure	3
2.1.3	Selection of Failure Modes	4
2.1.4	Statistical Life Prediction Model	4
2.1.5	Description of Failure Modeling	15
2.2	Combustor Failure Modes	21
2.2.1	Combustor Failure Mechanisms	21
2.2.2	Selection of Failure Modes	23
2.2.3	Description of Burner Failure Modeling	24
3.0	PHASE II - FORMULATION AND DEVELOPMENT OF MISSION ANALYSIS PROGRAM	54
4.0	PHASE III - VERIFICATION OF FAILURE MODELS	55
4.1	Model Calibration	55
4.1.1	Turbine Failure Model Calibrations	55
4.1.2	Combustor Failure Model Calibrations	56
4.2	Uncertainty Analysis	59
4.2.1	Turbine Airfoils	59
4.2.2	Burner Analysis	65
5.0	PHASE IV - MISSION MIX LIFE SENSITIVITY STUDY	68
5.1	Mission Analysis Life Prediction	68
5.1.1	Transport Mission	68
5.1.2	Fighter/Attack Mission	69
5.1.3	Mission Mix Sensitivity	70
	REFERENCES	72
	APPENDIX	73

LIST OF ILLUSTRATIONS

Figure No.	Subject	Page No.
1	Relationship Between Traditional Probability Displays and the Weibull Form	6
2	JT9D-7 First-Stage Turbine Blade Creep-Fatigue Interaction Failure	7
3	JT9D-7 First-Stage Turbine Blade Leading-Edge Oxidation/Corrosion/Erosion Failure	8
4	JT9D-7 Second-Stage Turbine Blade Creep-Rupture Failure	9
5	JT9D-7 Second-Stage Turbine Blade Creep-Fatigue Failure	10
6	TF30-P-100 First- and Second-Stage Turbine Blade Creep Scrap Life	11
7	TF30-P-100 Third-Stage Turbine Blade Creep Scrap Life	12
8	TF30-P-100 Second-Stage Turbine Blade Under-Shroud Cracking Scrap Life	13
9	TF30-P-100 Second-Stage Turbine Vane Coating Replacement Life	14
10	Input and Output for Turbine Failure Model	15
11	Nomenclature for Airfoil Creep Calculation	17
12	Creep Mode Model	18
13	Creep-Fatigue Interaction Mode Model	19
14	Erosion/Corrosion/Oxidation Mode Model	20
15	Typical Larson-Miller Parameter (LMP) Curve	21
16	Typical Curve of Cyclic Life vs. Total Strain Range	22
17	Typical Curve of Metal Temperature Effects on Coating	22
18	Axial Crack Frequency Study	23
19	Typical Stress-Strain-Temperature Relationship	25

LIST OF ILLUSTRATIONS (Cont'd)

Figure No.	Subject	Page No.
20	Typical Circumferential Cracks in Can-Annular Burner	26
21	Typical Axial Cracks in an Annular Liner	27
22	Relative Magnitude of Hoop and Bending Stress Components vs. Liner Radius	28
23	Typical Stress-Strain Hysteresis Loop	29
24	Typical LCF Life-Strain Log Plot With Langer's Hypothesis	31
25	Typical Log Plot of Stress-Strain Relationship in the Plastic Region	33
26	Creep Data - B_t Relationship	35
27	Graphical Description of Time-Hardening Theory	36
28	Combustor Louver Lip Buckling Nomenclature	37
29	Elastic Buckling Geometry Relationship	39
30	Critical Buckling Strain-Temperature Relationship	40
31	Typical Stress-Strain Curve For Lip Buckling Model	41
32	Thermal Buckling Deflection vs. Lip Strain	42
33	Critical Strain Range - Buckling Coefficient Relationship	43
34	Coating Induced Buckling Data	48
35	Estimated Hoop Restraint Factor on Axial Bending of Louver Lips Due to Coating Expansion	50
36	Oxidation-Deflection Constant	51
37	Maximum Oxidation Deflection	52
38	Coating-Induced Buckling Procedure	53
39	JT9D-7 Combustor - Comparison of Mission Life Predicted by Creep-LCF Failure Model with Field Service Data	56

LIST OF ILLUSTRATIONS (Cont'd)

Figure No.	Subject	Page No.
40	Comparison of Creep-LCF Life Prediction With Field Service Experience	57
41	Schematic of Fluidized Bed Test Rig for Obtaining Combustor Louver Lip Buckling Data	58
42	Calibration of Louver Lip Thermal Buckling Model	58
43	Design Application of Burner Failure Models - JT9D-70 Center Liner	60
44	Design Application of Burner Failure Models - JT9D-70 Inner Liner	61
45	Radial Gas Profile Shift	64

LIST OF TABLES

Table No.	Title	Page No.
1	Results of Airline Burner Survey for JT9D-7 Single Operator	24
2	Hastelloy X Properties Used to Calculate Thermal Buckling	45
3	Variables for Uncertainty Study	62
4	Turbine Uncertainty Analysis	63
5	Phase III Burner Cracking Model Uncertainty Analysis	66
6	Phase IV Burner Louver Lip Buckling Uncertainty Analysis	67
7	Hot Section Component Life Predictions (B-50 UER) For Transport (JT9D) Mission in Hours	69
8	Turbine Component Life Predictions (B-50 Scrap) For Fighter/Attack (TF30-P-100) Mission in Hours	69
9	Mission Parameter Sensitivity Study, JT9D-7 Hot Section Components	70
10	Mission Parameter Sensitivity Study, TF30-P-100 Turbine Components	71

SECTION 1.0

INTRODUCTION

Design specifications for all military aircraft engines include durability and life requirements for all hot section parts. The durability of hot-section parts is highly dependent on the type of aircraft mission flown, the geographical location of the operating base, and pilot operation since all these factors affect the temperature-pressure environment in the hot section and the cyclic history of the parts.

An accurate, realistic, mission-analysis-oriented, life prediction system for the combustor and the turbine can reduce development and maintenance costs of a new engine or advanced model of a current engine. Such a system can improve combustion and turbine durability design capability, provide a method for defining realistic accelerated endurance tests which simulate design missions, and evaluate component life as a function of actual use in the field for maintenance and logistic considerations.

This report describes the analytical development of a computer program for predicting the service lives of combustors and turbine airfoils as functions of aircraft mission parameters. The work effort was organized in four phases. Phase I involved the gathering of data from field service and in-house testing, the identification of the combustor and turbine airfoil failure modes, and the development of failure models based upon the physical processes involved and calibrated with the available data. In Phase II, a mission analysis program, currently used to predict turbine airfoil lives, was updated to reflect the most recent turbine service data and modified to accept the burner failure models developed in Phase I.

The results of Phases I and II were verified in Phase III using available service data. The uncertainty of the model was established by determining the sensitivity of the predicted service life of the component to variations in material data, thermal gradients and manufacturing tolerances. In Phase IV, a mission mix life sensitivity study was conducted using a base mission and three alternate missions. The B-50 lives (time period during which 50 percent of the components will have failed) of the turbine airfoils were predicted for both a transport and fighter/attack propulsion system.

The work accomplished in each phase of this program is discussed in separate sections below.

SECTION 2.0

PHASE I – IDENTIFICATION AND MODELING OF COMBUSTOR AND TURBINE AIRFOIL FAILURES

2.1 TURBINE AIRFOIL FAILURE MODES

2.1.1 Turbine Airfoil Failure Mechanism Review

Today's modern gas turbine engines with their high thrust-to-weight ratio and low specific fuel consumption are comprised of many sophisticated components utilizing the latest in high-strength materials and technology. This is especially true in the turbine component where the latest super-alloys with special protective coatings are used in an environment with gas temperatures well above the melting point of the materials. Today's turbine airfoils must endure higher temperatures, higher stresses, and more severe transients than ever before. These severe operating conditions have resulted in three primary modes of failure in turbine airfoils. These modes are creep, creep-fatigue interaction, and oxidation/corrosion/erosion.

Creep causes failures by having the part either rupture or exceed allowable dimensions. Creep stress is generally due to three causes, all of which may be present in a turbine airfoil. These causes are thermal gradients, rotation, and airflow. Thermal gradients occur primarily in cooled parts where a difference in metal temperature between elements of the part establishes strain in those elements, causing creep. Rotation causes a centrifugal stress in turbine blades, and airflow causes bending stresses in both vanes and blades. These stresses, coupled with high metal temperatures, are the forcing functions in the creep phenomenon. The amount of creep damage which a blade or vane has sustained is measurable with special gages that measure blade growth or vane deflection. At this time, no method has been developed for production use that will refurbish material that has sustained creep damage. For this reason, a turbine blade that has undergone creep growth beyond limits must be scrapped. However, creep deflections on less critical airfoils, such as vanes, have been refurbished in some instances. Vane trailing edge bow is an example of a repairable creep failure. Vanes which have this type of failure mode will usually have both repairable limits and scrap limits. UER's (Unscheduled Engine Removals) can be caused by the creep failure mode, that is, by having a blade reach creep rupture.

The creep-fatigue interaction mechanism results in failure by the development of cracks on the surface of the airfoil (either inner or outer surface of a cooled airfoil). Creep-fatigue interaction can be described in terms of the exhaustion of material ductility at the critical location on the airfoil surface. In this model, strain is introduced as described above, and also by cyclic stresses resulting from transient engine operation. Rapid acceleration or deceleration of the engine results in severe cyclic strains especially in cooled airfoils. Cracks due to creep-fatigue interaction which occur on less critical components, such as vanes, are often repairable. Cracks which occur in critical areas of turbine vanes or turbine blades cannot be repaired and therefore cause the part to be scrapped. Cracks which occur in critical areas often progress to rupture before they are discovered and thereby cause a UER.

The oxidation/corrosion/erosion mode results in failure by the depletion of the airfoil coating and/or base material. Oxidation is the reaction of oxygen in the gas stream with various elements of the alloy, thereby depleting and weakening the alloy. Corrosion in turbine airfoils results from airborne salts or sulfur compounds in the fuel reacting with the airfoil coating and/or elements in the airfoil alloy. The sodium sulfate deposits on the airfoil and reacts with those elements which were added to the alloy to impart oxidation resistance, thereby reducing the inherent oxidation resistance of the alloy. The erosive nature of the turbine atmosphere is produced by small particles of carbon formed in the burner and other fragments of upstream material which are carried by the gas stream to the turbine airfoils at high temperatures and high velocities. The loss of metal due to erosion can be significant over the life of a turbine part, but, perhaps more important, the loss of protective coating through erosion renders the alloy vulnerable to attack through oxidation and corrosion. Analytical models of these phenomena are the least developed of all failure modes at this time and generally must be dependent on empirical data. Since all three of these mechanisms usually occur simultaneously in varying degrees, one model which correlates coating life to metal temperature is used for all failures of this type.

Coating and base metal depletion within specified limits are repairable by a strip and recoat process on both blades and vanes. Airfoils which have metal loss beyond repairable limits must be scrapped. This failure mode can lead to blade rupture by reducing the load-carrying capability of the airfoil or by providing a flaw from which a crack may initiate and propagate.

2.1.2 Definition of Failure

A turbine airfoil may be considered failed in three ways: (1) inspection of an airfoil may reveal damage which is beyond allowable replacement limits and therefore must be repaired, (2) inspection of an airfoil may reveal damage which is beyond repairable limits and therefore must be scrapped, and (3) an airfoil may sustain damage which causes it to rupture and thereby results in an unscheduled engine removal (UER). The ruptured airfoil is by far the most critical type of failure since it often results in an inflight shutdown of the engine.

A new inspection technique has been developed and used on the Pratt & Whitney Aircraft JT9D engine. This inspection technique makes use of a boroscope probe to look into the engine hot section while the engine remains installed in the aircraft. Whereas in the past an engine was either removed for a scheduled inspection or for a UER caused by the failure of some component, an engine can now be removed based on results observed with the boroscope. This type of failure can be caused by any of the three primary turbine airfoil failure modes since creep and creep-fatigue interaction can lead to a crack before the airfoil actually ruptures. There have also been numerous instances where oxidation/corrosion erosion distress on a turbine blade has been discovered by the boroscope inspection, thereby resulting in a UER but preventing further damage by a blade rupture. Hence, the boroscope inspection introduces a new type of UER failure for turbine airfoils — removal for visual distress.

2.1.3 Selection of Failure Modes

The selection of failure modes for analysis in this program was based upon the relative importance of the mode to the reliability of the respective engine and on the availability of data to substantiate the model. The JT9D-7 and the TF30-P-100 have been selected as representative of transport and fighter attack engines. For the JT9D-7, the failure modes selected were those that caused unscheduled engine removals (UERs). These types of failures are extremely important to an operator and extensive data is available for the JT9D-7 engine. The TF30-P-100 engine, on the other hand, has not accumulated any UER data for turbine airfoil failures. Therefore, scrap modes from this engine were selected for analysis. A list of the failure modes selected for analysis is summarized in the following table:

JT9D-7		
1st vane	(creep-fatigue cracking)	UER
1st blade	(creep-fatigue cracking)	UER
1st blade	(oxidation/corrosion)	UER
2nd vane	(creep-fatigue cracking)	UER
2nd blade	(creep-rupture)	UER

TF30-P-100		
1st vane	(creep-fatigue cracking)	scrap
1st blade	(creep)	scrap
2nd blade	(creep)	scrap
2nd blade	(under shroud cracking)	scrap
3rd blade	(creep)	scrap
2nd vane	(oxidation/erosion)	scrap and refurbishment

These failure modes have been selected as pertinent examples. They are not meant to be all inclusive. The user can analyze other failures in these or other engines by incorporating the failure routines in the mission analysis program.

2.1.4 Statistical Life Prediction Model

The statistical model used at Pratt & Whitney Aircraft is based on the Weibull method of failure analysis.

The Weibull method is a statistical presentation and analysis technique which permits the use of failure and non-failure (suspension*) data to determine a probability distribution via the Weibull equation:

$$F(t) = 1 - e^{-\left(\frac{t-t_0}{\eta}\right)^\beta} \quad (1)$$

*Refers to unfailed parts in service that have not yet accumulated as much time as some of the failed parts.

where	$F(t)$	=	cumulative probability of failure (the area under the distribution from t_0 to t)
	β	=	Weibull slope
	η	=	characteristic life
	t	=	random variable (stress, time, etc.)
	t_0	=	origin of the distribution

The probability density function $f(t)$ is equal to $dF(t)/dt$, the ordinate of the frequency distribution

$$f(t) = \frac{\beta (t-t_0)^{\beta-1}}{\eta^\beta} e^{-\left[\frac{\beta}{\eta}(t-t_0)\right]} \quad (2)$$

Presentation of the Weibull analysis requires special probability graph paper: the ordinate is a double log scale of the expression containing the "fraction failing" while the abscissa is a single log scale of the random variable. The relationship between traditional probability displays and the Weibull form is shown in Figure 1. It may be seen that the Weibull line is, in fact, a distribution. The slope, β , is a shape factor since it indicates the skewness of the probability density function. The characteristic life, η , is frequently not used in practice due to the lack of convenient mathematical interpretation. In its place, the median life, i.e. the life at 50 percent cumulative probability, is used — this life is often referred to as the "B-50 life".

Presentation of data in the Weibull manner allows the uniform presentation and easy interpretation of statistical data. By routinely analyzing data and incorporating new data in this manner, ready access to a vast data bank is provided. Data available encompasses turbine vanes and blades further separated by failure mode and operator for each engine model. This data varies somewhat due to engine maturity and operator experience, and is limited in many cases where no failure experience exists.

Figures 2 through 9 are samples of the statistical models used at Pratt & Whitney Aircraft for several turbine failure modes of the JT9D-7 and TF30-P-100 engines. The JT9D Weibull plots have been updated since the first interim report (Ref. 1). The JT9D-7 first blade creep-fatigue interaction failure mode is shown in Figure 2; JT9D-7 first blade leading edge oxidation/corrosion/erosion failure mode is shown in Figure 3; the JT9D-7 second blade creep-rupture failure mode is shown in Figure 4 and the second stage creep-fatigue failure mode is shown in Figure 5. As additional reports of UER failures for each particular mode are received, the Weibull analyses are periodically revised to reflect all of the available data.

Figures 6 through 9 are the statistical models of several TF30-P-100 turbine failure modes for full power operation of the engines. Service failure data on the P-100 engines does not exist at this time, since these engines have only accumulated a maximum of 600 hours in service. The accumulation of data is also complicated by the fact that these engines are being operated at reduced power, and approximately 300 to 400 of the 600 hours were accumulated at reduced power operation. For this reason, the damage sustained by the turbine airfoils is well below what would be expected at 600 hours. Due to the lack of service failure data, the statistical models shown for the P-100 engine are a result of calculating the B-50 life and using a Weibull slope which is based upon the limited amount of low time (200 to 300 hours) growth data on first-stage blades. The calculation of the B-50 life was accomplished with the use of the mission analysis program and a physical failure model which has been calibrated by in-house endurance engine data. Until more time is accumulated on these engines, it will be impossible to develop a statistical model based on service failure data.

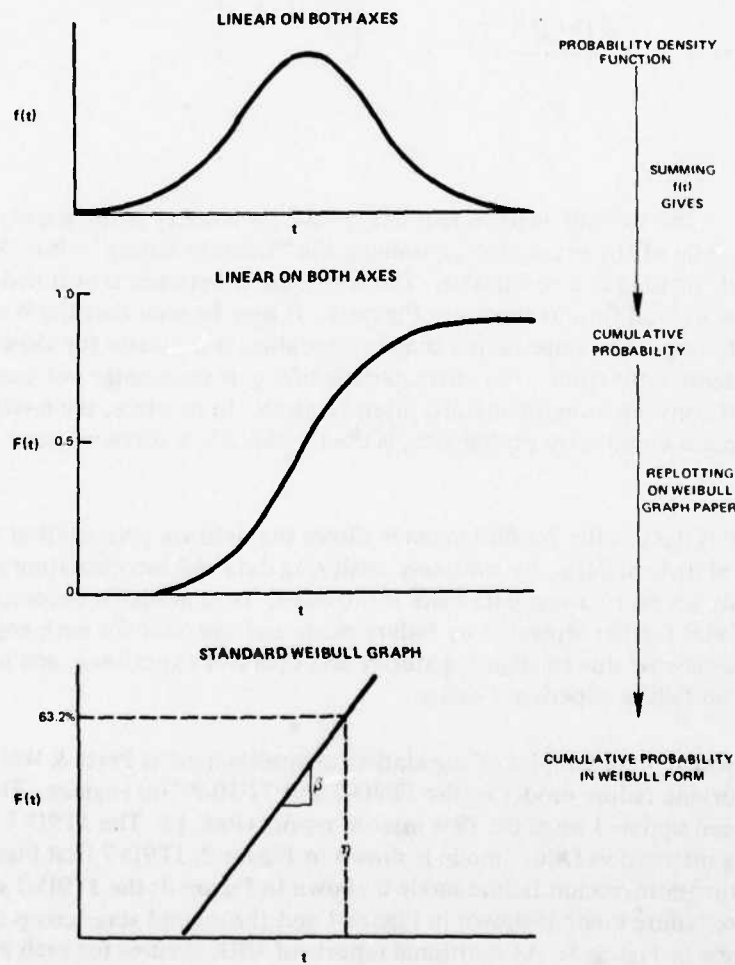


Figure 1 Relationship Between Traditional Probability Displays and the Weibull Form

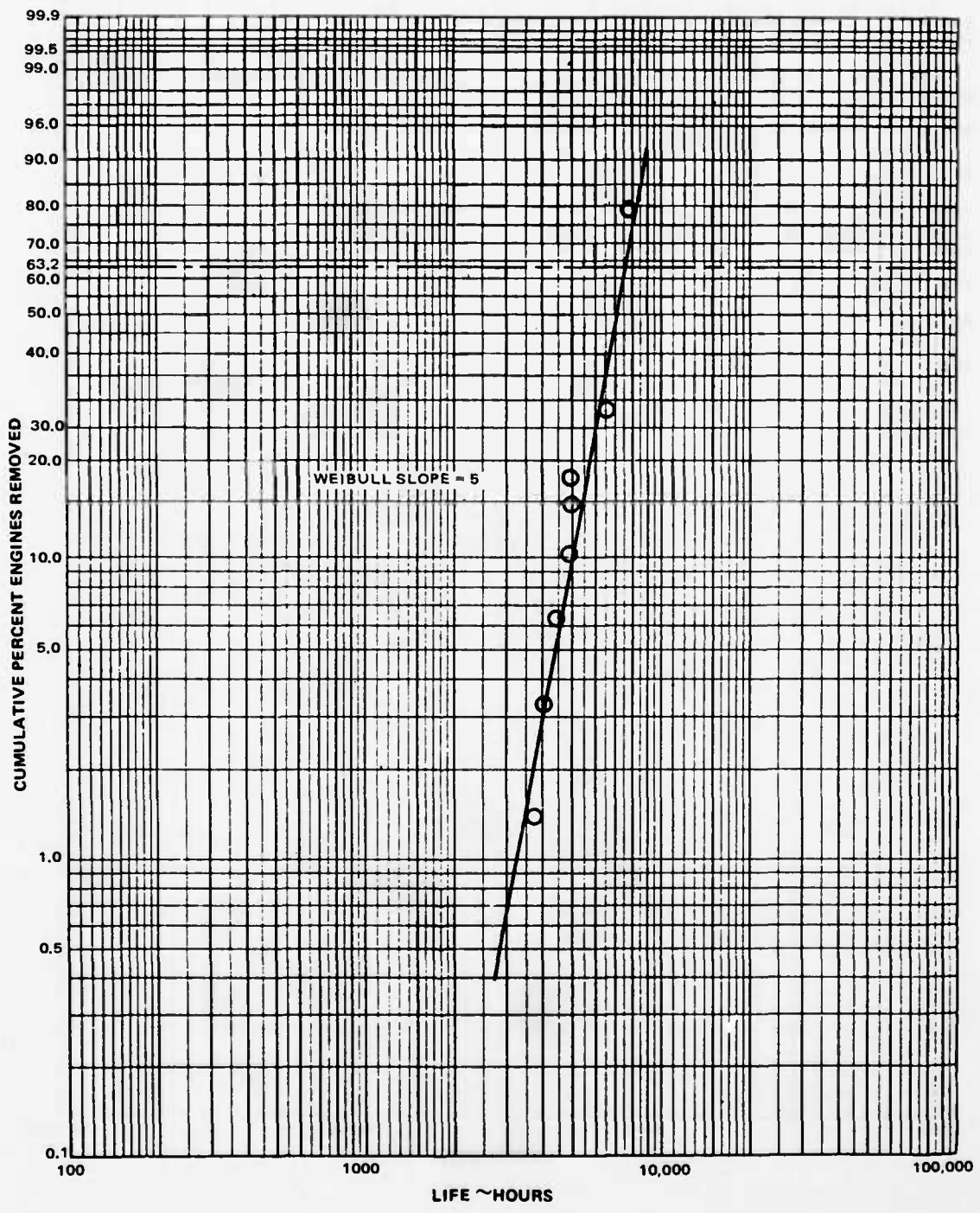


Figure 2 JT9D-7 First-Stage Turbine Blade Creep-Fatigue Interaction Failure

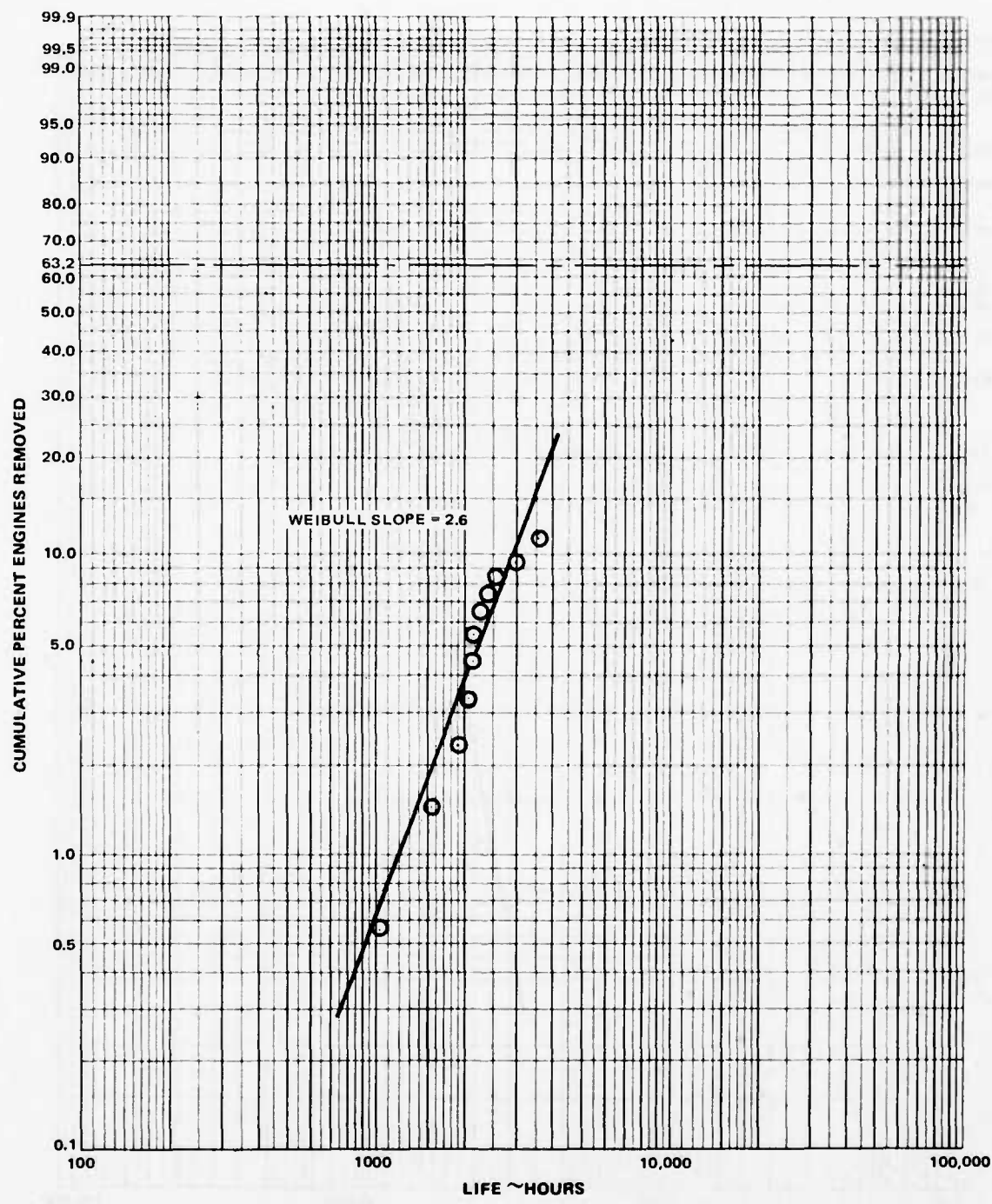


Figure 3 JT9D-7 First-Stage Turbine Blade Leading-Edge Oxidation/Corrosion/
Erosion Failure

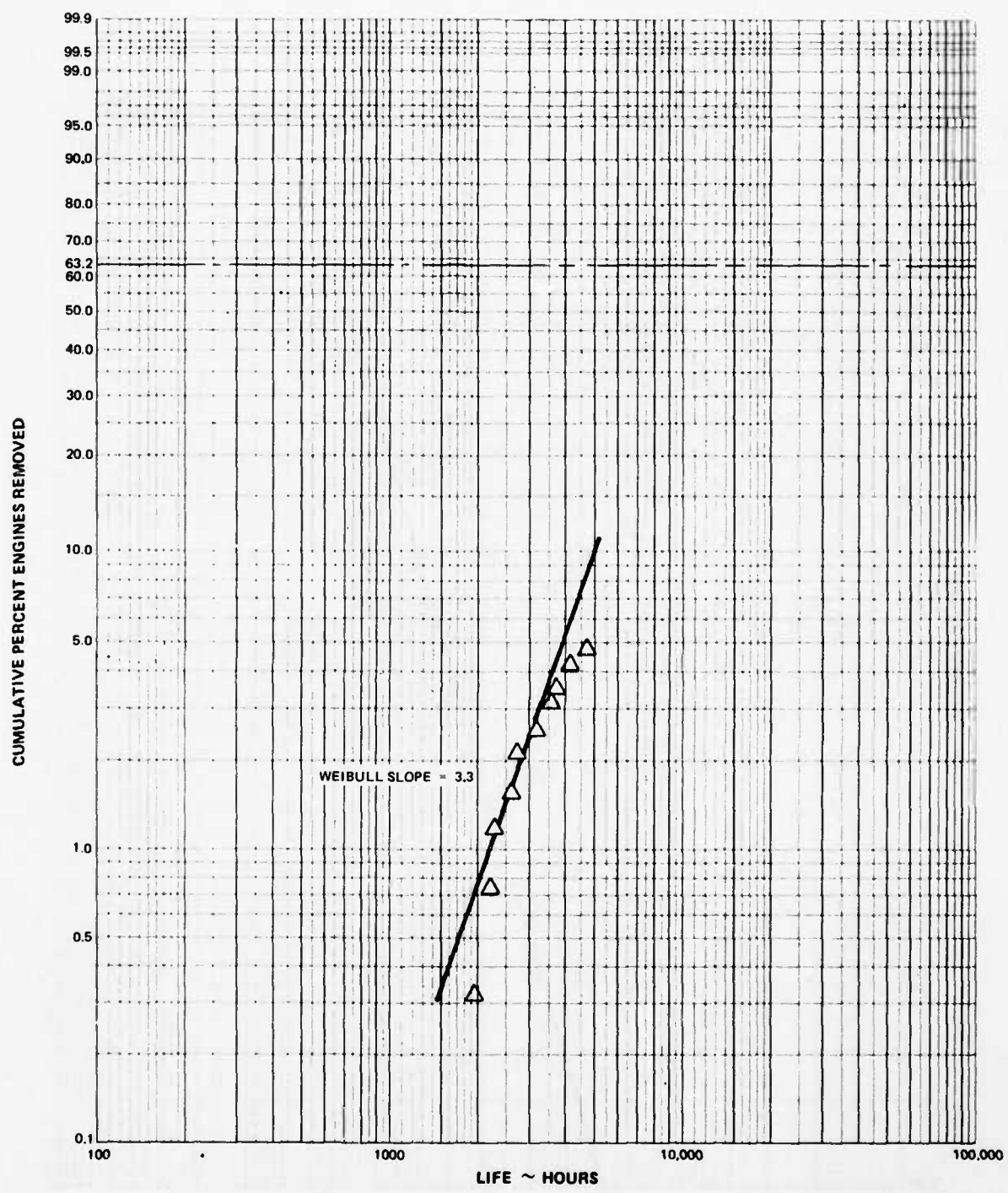


Figure 4

JT9D-7 Second-Stage Turbine Blade Creep-Rupture Failure

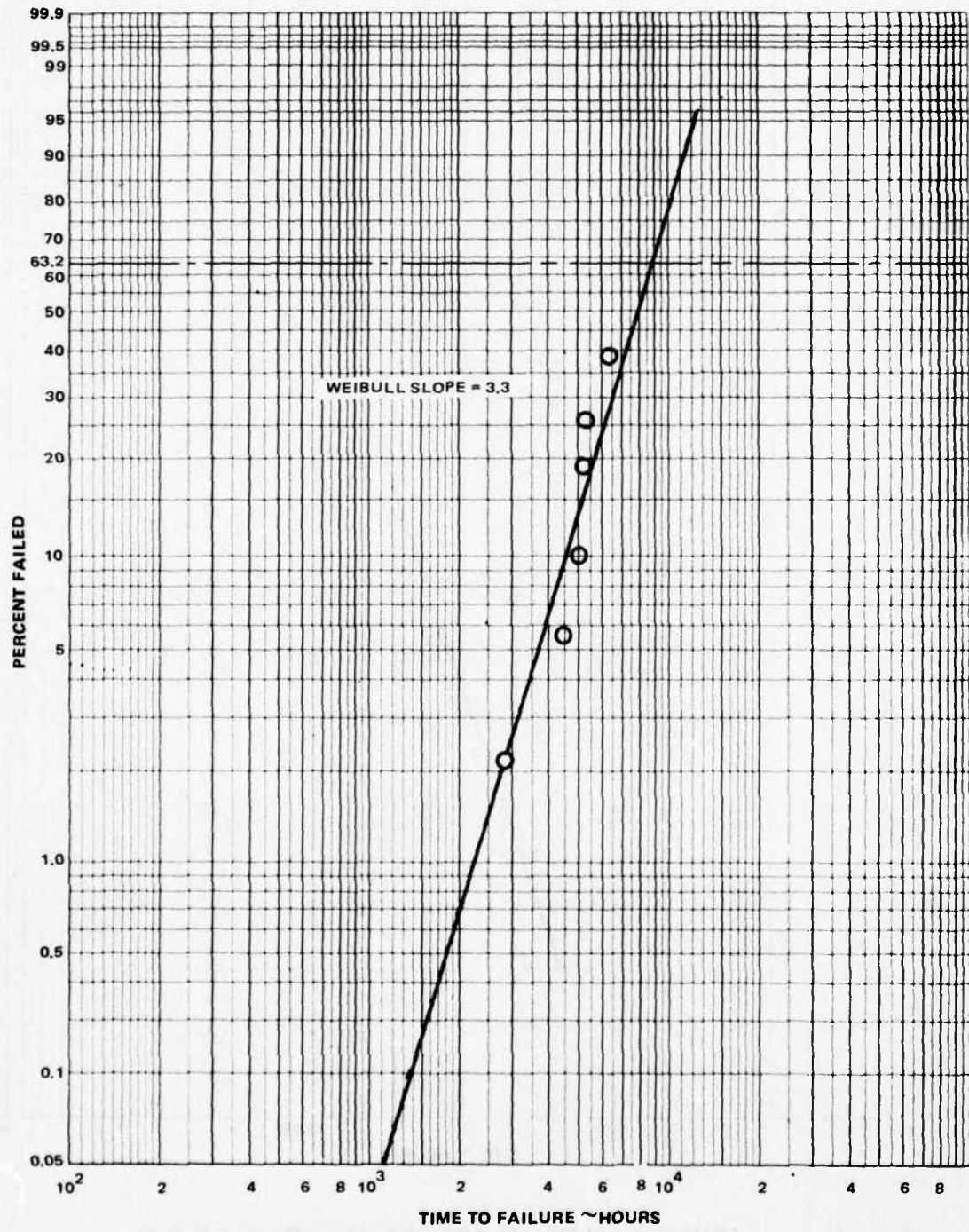


Figure 5 JT9D-7 Second-Stage Turbine Blade Creep Fatigue Failure

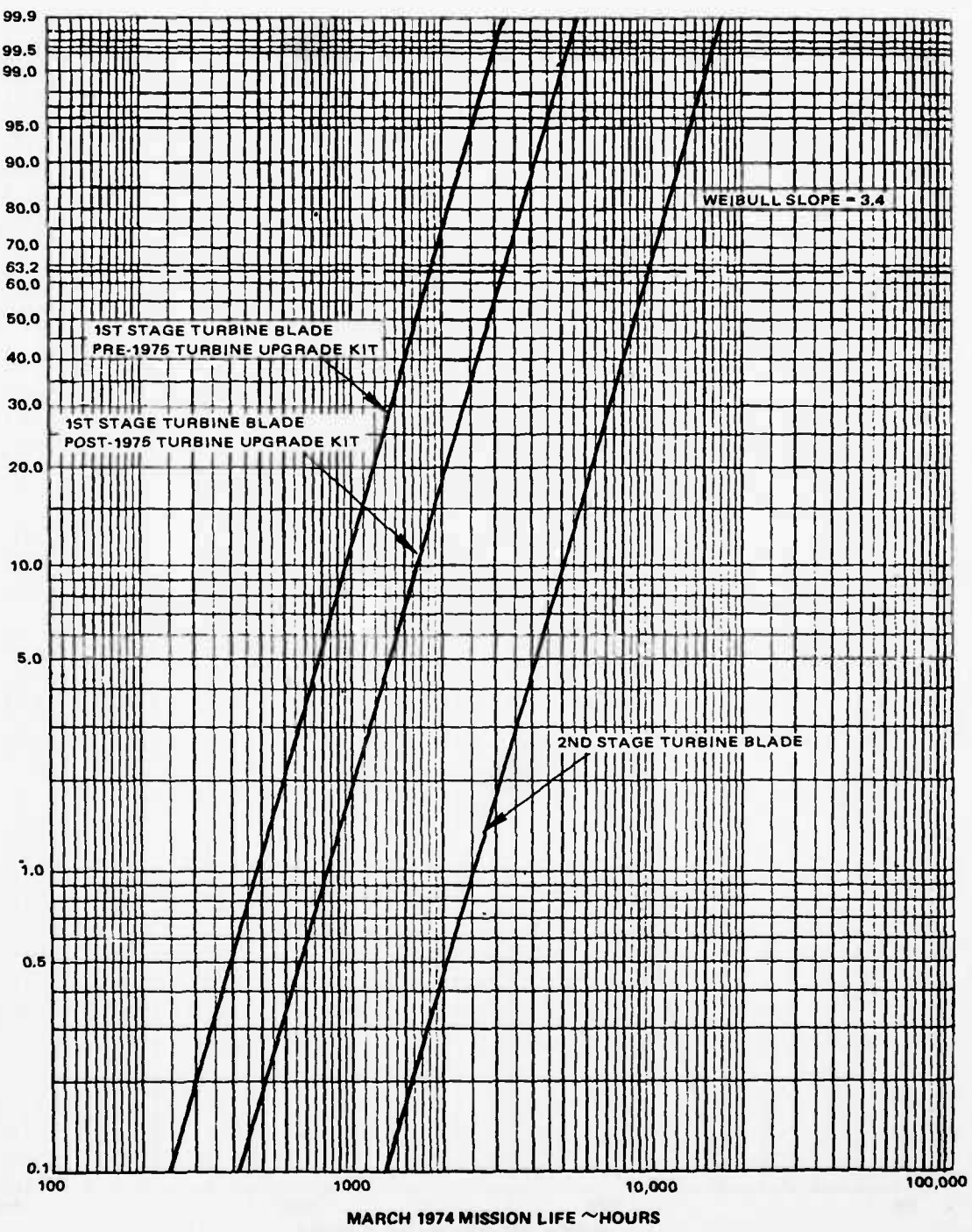


Figure 6 TF30-P-100 First and Second-Stage Turbine Blade Creep Scrap Life

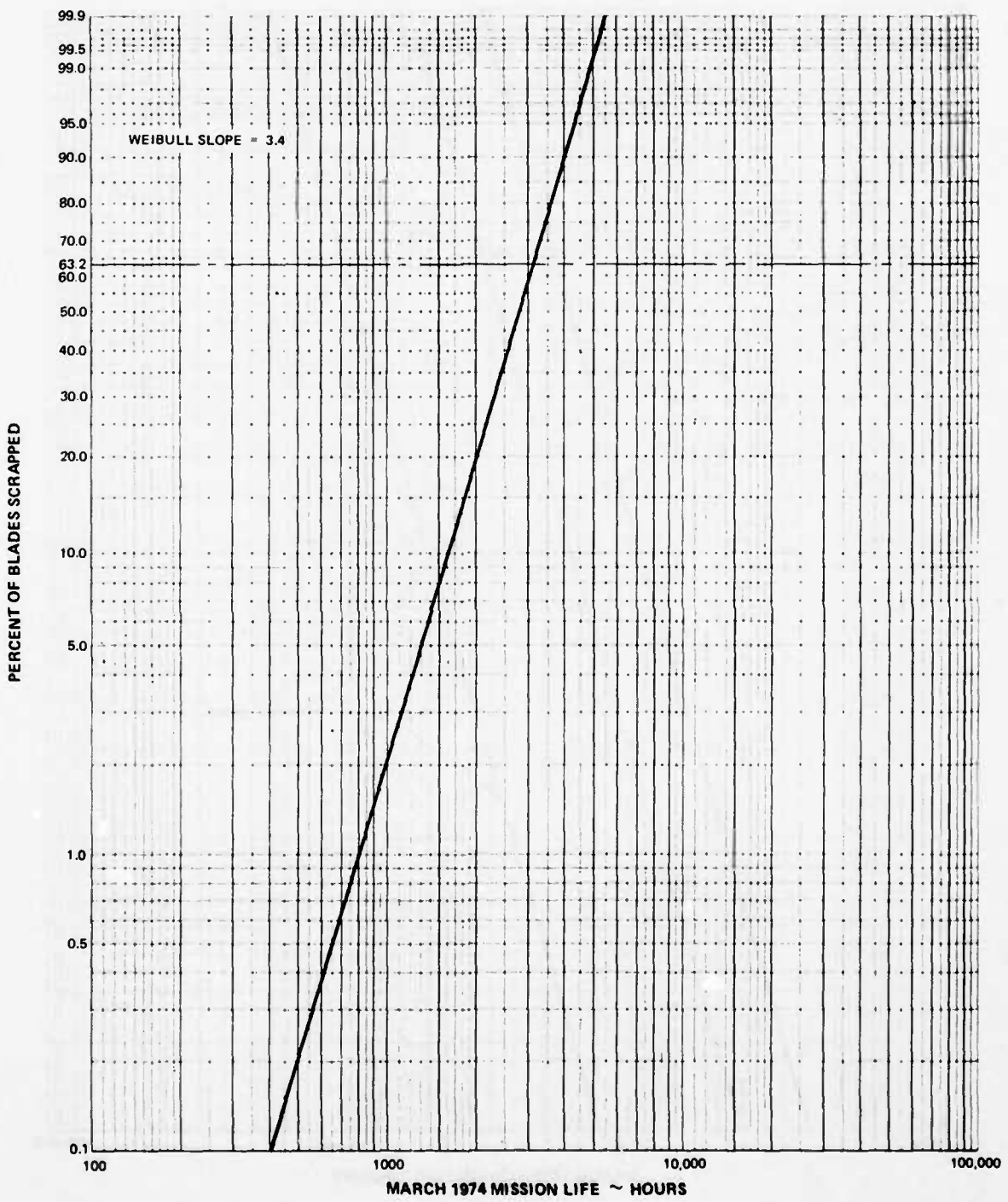


Figure 7

TF30-P-100 Third-Stage Turbine Blade Scrap Life

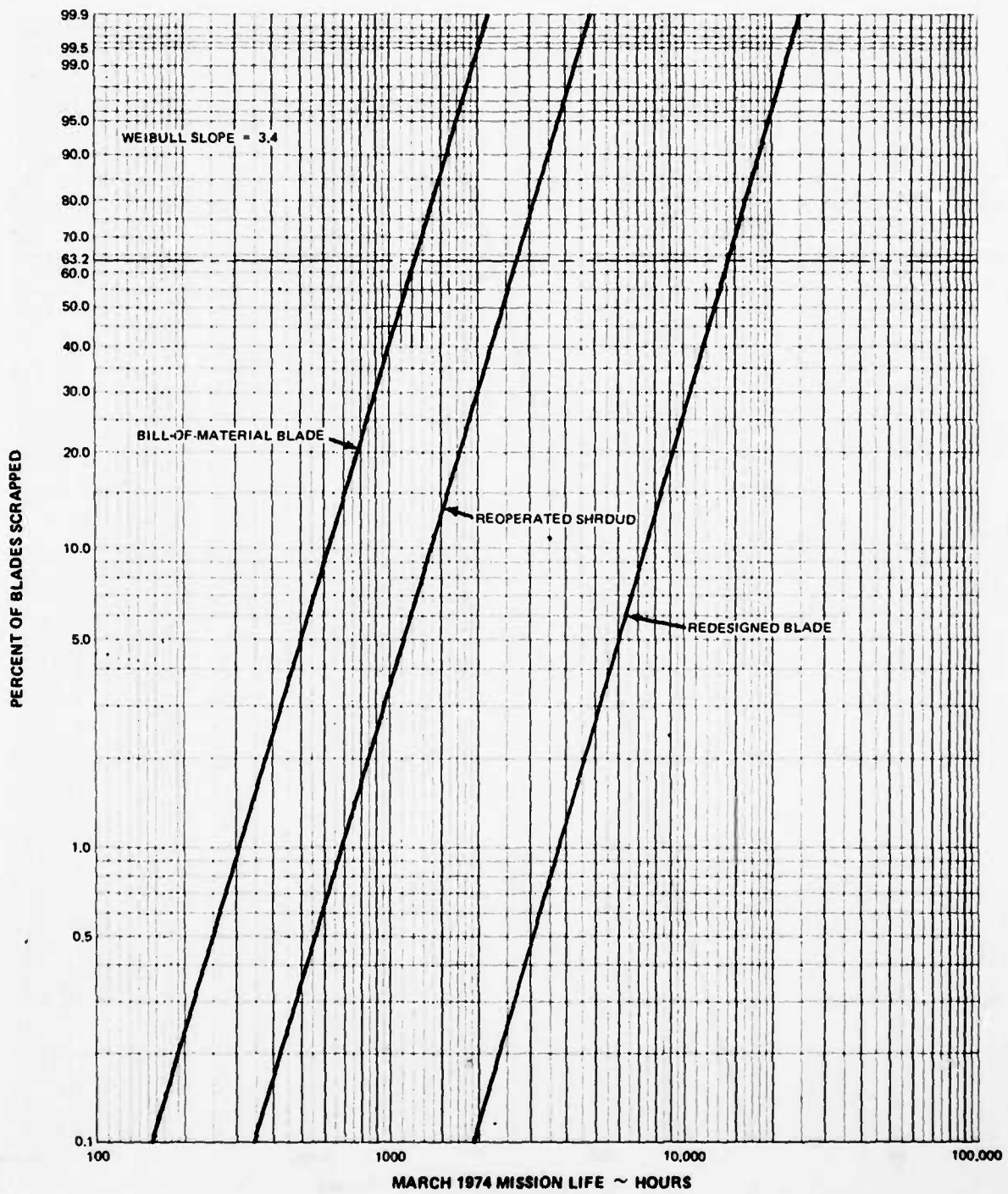


Figure 8 TF30-P-100 Second-Stage Turbine Blade Under-Shroud Cracking Scrap Life

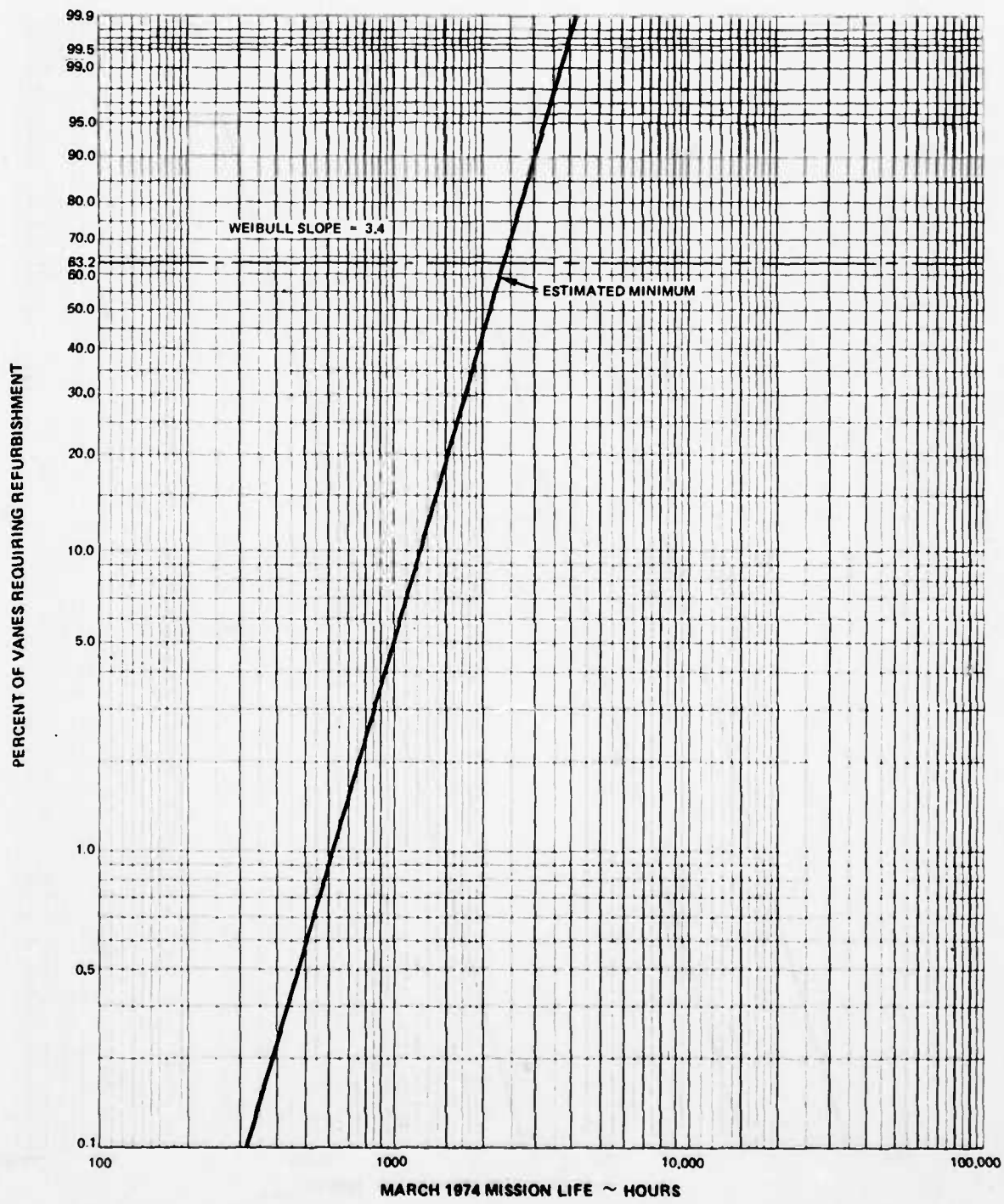


Figure 9 TF30-P-100 Second-Stage Turbine Vane Coating Replacement Life

2.1.5 Description of Failure Modeling

A turbine life prediction model is currently operational at Pratt & Whitney Aircraft. This model considers the general failure processes of creep, fatigue, and oxidation/erosion/corrosion as may be manifested by component stretch, deflection, cracking and burning to name a few of the more predominant failure identifications. This model is general enough to analyze vanes and blades, cooled and uncooled, with and without coatings on all engine types.

The failure model is shown schematically in Figure 10. The input parameters required from the engine performance and mission definition are engine station pressure near the part, coolant supply temperature, engine station temperatures on either side of the part, rotor speed, and mission time spent at the power level. In addition, the results of a reference point analysis are required to give metal temperature, stress, and strain range for critical regions of the point defined at a reference power level. This reference point analysis is performed externally to this mission analysis/physical modeling system and the results must be provided as input. This analysis consists of a heat transfer and stress analysis for a typical power setting as well as for a typical transient excursion. The results are used as input to the program and are in the form of stress, temperature, and strain range for all critical elements of the part as required for each failure mode.

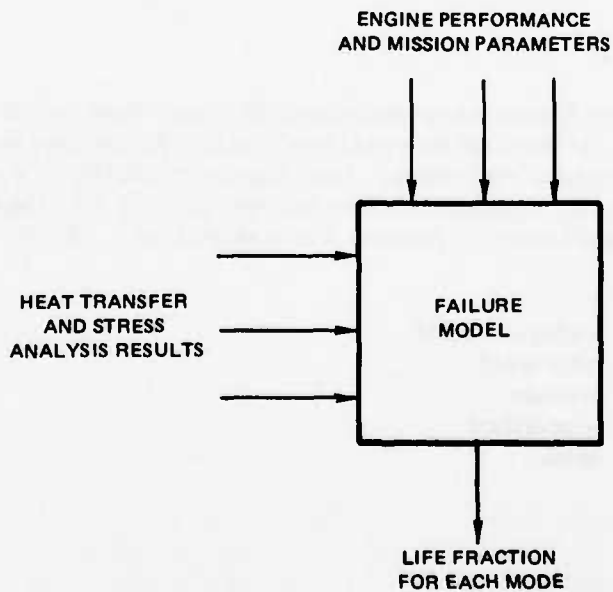


Figure 10 Input and Output for Turbine Failure Model

The general procedure followed by the mission analysis is to break the mission into a series of steady-state performance points and a series of transient cycles. The failure model takes these increments and calculates a life for each. This "life" is the full expectancy of the part assuming only this single performance point is run until failure. At the end of the mission the life fraction rule is applied for creep, fatigue, and erosion/corrosion/oxidation while creep-fatigue interaction is used when required. The life fraction rule (often called Miner's rule) is used to combine differing creep, fatigue, or erosion/corrosion/oxidation damage rates by weighting each rate by the time spent at that rate. Since these rates are related to the life expectancy for each performance point, the life fraction rule may be stated as follows:

$$L = \frac{\sum_{i=1}^n t_i}{\sum_{i=1}^n t_i/L_i} \quad (3)$$

where L is the average life
 t_i is the time spent at the i^{th} performance point
 L_i is the life expectancy at the i^{th} performance point

2.1.5.1 Turbine Creep Life

The creep failure model requires a metal temperature and stress at each flight condition. Calculation of metal temperature and stress for the power level is made by scaling the known reference point analysis by the engine performance. This temperature and stress are used with material properties according to the equations below to calculate the creep life. The inclusion of mission time yields the required creep life fraction. The nomenclature is tabulated below and described in Figure 11.

C_a, C_b, C_c	= scaling constants
N	= rotor speed
P	= pressure
T	= temperature
σ	= stress

Subscripts

C	= coolant
G	= gas
M	= metal
N	= rotor speed component
P	= pressure component
R	= reference
S	= supply
1	= station inlet
2	= station exit

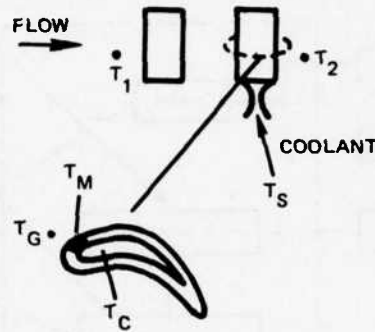


Figure 11 Nomenclature for Airfoil Creep Calculation

Three input scaling constants, relating the various temperatures are defined as:

$$C_a = \frac{T_M - T_C}{T_G - T_C} \quad (4)$$

$$C_b = \frac{T_G - T_2}{T_1 - T_2} \quad (5)$$

$$C_c = \frac{T_C - T_G}{T_G - T_S} \quad (6)$$

The metal temperature can then be related to the environmental temperatures and scaling factors by combining equations (4), (5) and (6). The resulting relationship is:

$$T_M = C_a [T_2 + C_b (T_1 - T_2)] + 1 - C_a \quad T_S + C_c \{ [T_2 - C_b \\ (T_1 - T_2) - T_S] \} \quad (7)$$

The stress is related to reference conditions by:

$$\sigma = \sigma_p \frac{P}{P_R} + \sigma_N \left(\frac{N}{N_R} \right)^2 \quad (8)$$

The stress and temperatures are used with the material property library to obtain a creep life for that flight increment. Figure 12 is a flow diagram for the turbine creep life model.

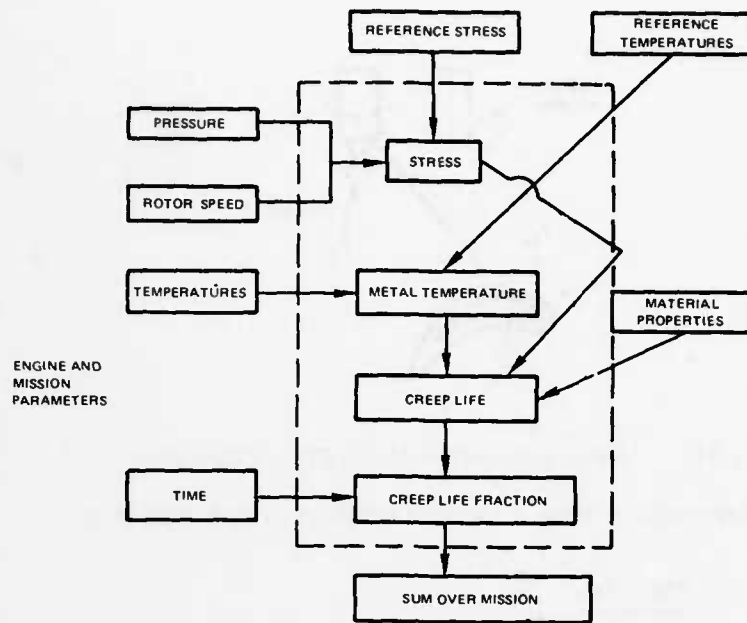


Figure 12 Creep Mode Model

2.1.5.2 Turbine Creep – Fatigue Interaction Life

The creep-fatigue interaction model employs a ductility exhaustion mechanism to combine creep and fatigue damage (Ref. 2). A total strain range is based upon input reference conditions (subscript R) and mission take-off conditions (nomenclature appears in previous section):

$$\Delta\epsilon_{TR} = \Delta\epsilon_{TRR} \frac{T_1 - T_S}{T_{IR} - T_{SR}} \quad (9)$$

The general form for the equation relating strain range ($\Delta\epsilon_{TR}$) and the number of cycles to failures as:

$$N_o = \frac{1}{4} \left(\frac{2\epsilon_f}{\Delta\epsilon_{TR}} \right)^a \quad (10)$$

If the component is strain cycles through n cycles ($n < N_o$), the ductility is reduced by:

$$\Delta\epsilon = \epsilon_f \left\{ 1 - \left[1 - 4n \left(\frac{\Delta\epsilon_{TR}}{2\epsilon_f} \right)^a \right]^{1/a} \right\} \quad (11)$$

In order to determine the interaction of fatigue and creep, the assumption is made that, for a given temperature and stress level the creep behavior of a material may be represented by the equation:

$$\epsilon_{CR} = At^b \quad (12)$$

Equating the failure mechanisms for creep and fatigue by saying that both contribute to a "reduction of ductility", it is possible to write an equation for an equivalent creep time based on the reduction of ductility during the fatigue portion of the cycle.

$$t_{eq} = \left(\frac{\Delta\epsilon}{A} \right)^{1/b} \quad (13)$$

The remaining ductility after a subsequent creep exposure of duration t_{inc} will then be

$$\epsilon_f' = \epsilon_f - A(t_{inc} + t_{eq})^b \quad (14)$$

Substitution of ϵ_f' , as calculated in Equation (14), into Equation (11) will then determine $\Delta\epsilon$ for the next n cycles. For the second and subsequent fatigue and creep exposures, t_{eq} takes the form

$$t_{eq} = \left(\frac{\Delta\epsilon + \epsilon_f - \epsilon_f'}{A} \right)^{1/b} \quad (15)$$

The above procedure is repeated until failure occurs, i.e., when

$$1 \leq 4n \left(\frac{\epsilon_{TR}}{2\epsilon_f} \right)^a \quad (16)$$

The creep-fatigue interaction model is shown schematically in Figure 13.

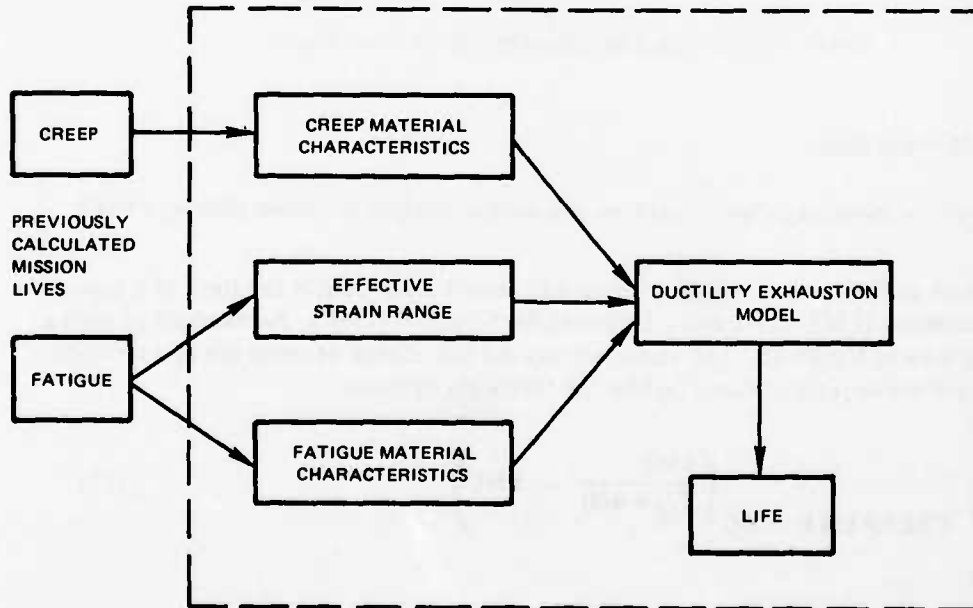


Figure 13 Creep-Fatigue Interaction Mode Model

2.1.5.3 Turbine Oxidation/Erosion/Corrosion Life

Temperatures calculated for the creep life (Section 2.1.5.1) are used to calculate oxidation/erosion/corrosion life from tables that are built into the deck. There is an option for the user to input these curves. The calculation procedure is illustrated in Figure 14.

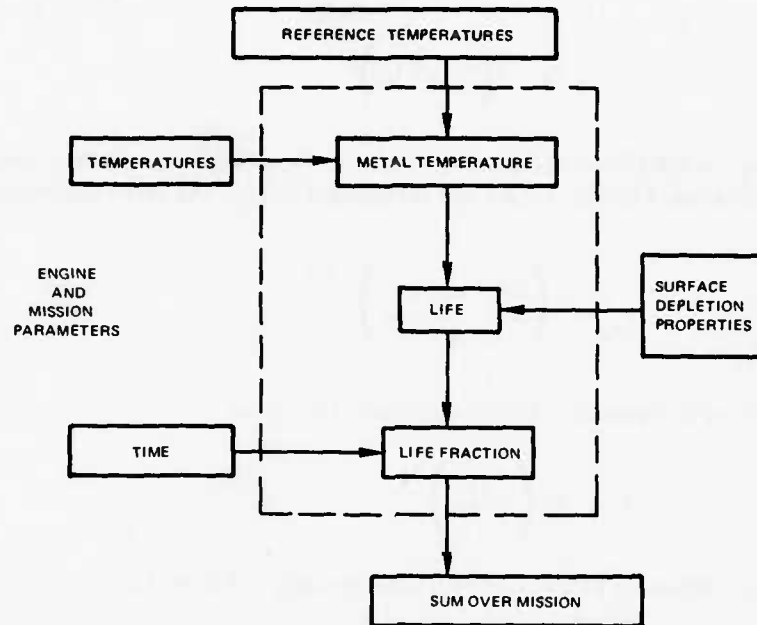


Figure 14 Erosion/Corrision/Oxidation Mode Model

2.1.5.4 Material Data

Three types of material property data are required to analyze the three primary failure modes.

The mission analysis program is programmed to accept creep data in the form of a Larson-Miller Parameter (LMP) curve and a Larson-Miller Constant (LMC). An example of such a curve is shown in Figure 15. This curve permits the calculation of creep life as a function of stress and metal temperature (T_M) by the following equation.

$$\text{CREEP LIFE} = 10 \left(\frac{\text{LMP}}{T_M + 460} - \text{LMC} \right) \quad (17)$$

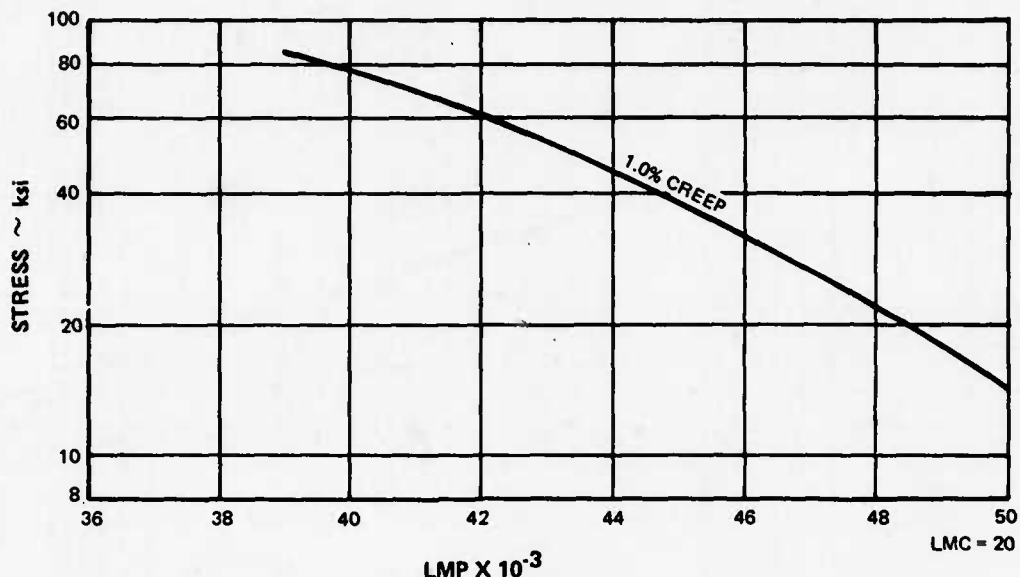


Figure 15 Typical Larson-Miller Parameter (LMP) Curve

A more extensive explanation of this method of data presentation can be found in section 2.2.3.3.4.

The creep fatigue interaction mode of failure requires fatigue data as well as the creep data. Fatigue data is input to the program in the well known Coffin-Manson format, that is, cycles to failure versus total cyclic strain represented by a straight line on log-log scales. An example of this data is shown in Figure 16.

Surface depletion properties vary with base metal as well as coating. The surface depletion properties are also input to the program in a similar manner. In this case, life is an exponential function of metal temperature. An example of this data is shown in Figure 17.

2.2 COMBUSTOR FAILURE MODES

2.2.1 Combustor Failure Mechanisms

Identification of burner failures and failure mechanisms is complicated by the non-critical nature of most burner failures and by the interaction of more than one failure mechanism. Blade rupture will result in an unscheduled engine shutdown, and a disk rupture is catastrophic. Consequently the failure criteria associated with these parts must be closely related to their ability to continue functioning. To relate some burner failure criteria, such as crack length or burned area, to the ability of the burner to function is far more difficult. There are examples of engines performing with "failed burners" undetected until a routine inspection or the failure of another component. The consequences of a burner failure are generally more economic than operational and result in a general deterioration of the engine or possibly serious damage to the turbine.

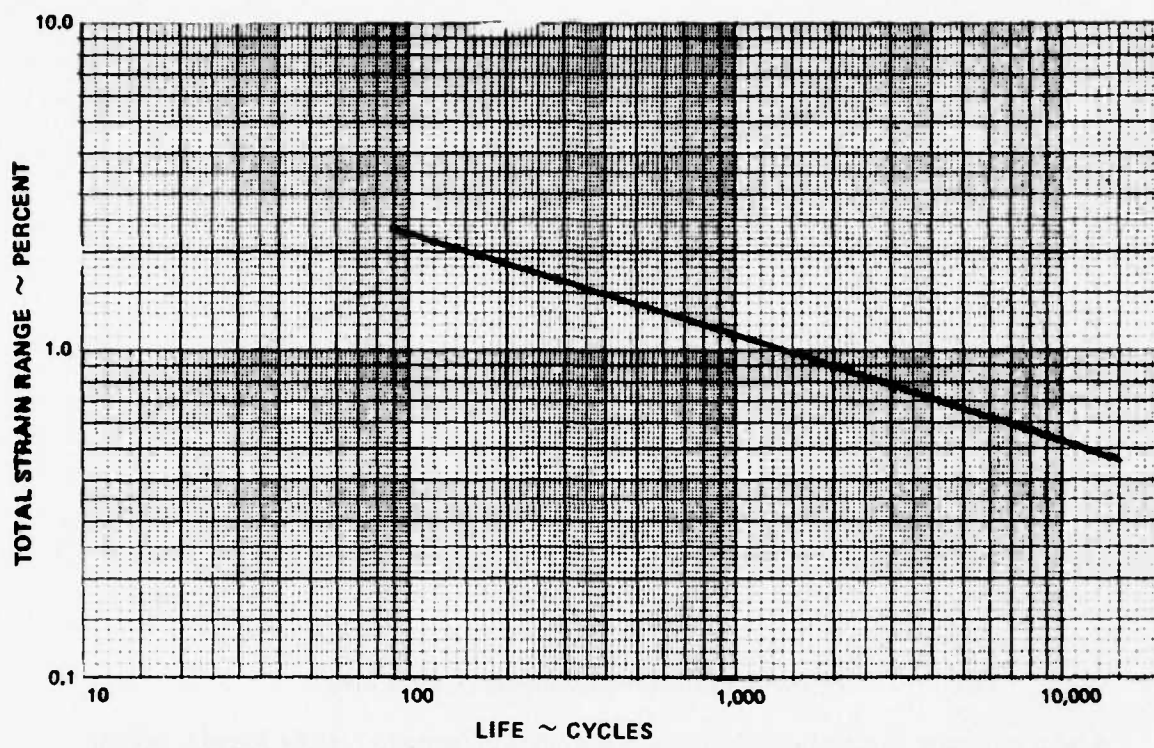


Figure 16 Typical Curve of Cyclic Life vs. Total Strain Range

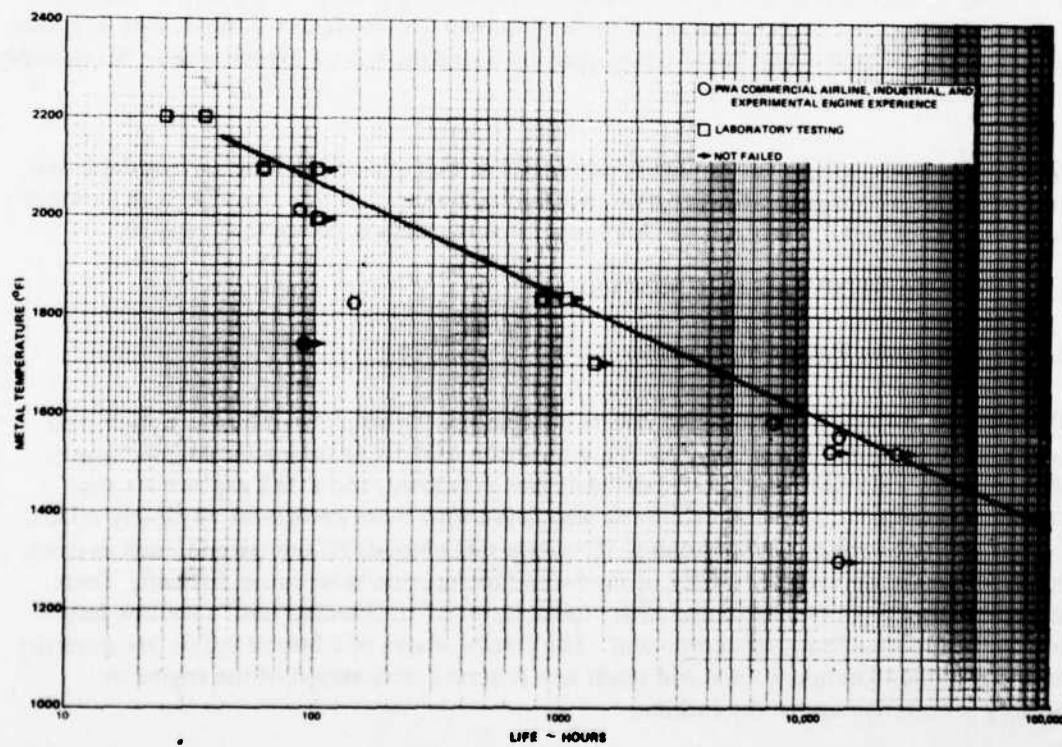


Figure 17 Typical Curve of Metal Temperature Effects on Coating

If the burner failure is non-critical, the reported time of the failure is really the observed time and may be related to overhaul schedules or the life of another component. If the failure of another component causes an engine removal, the burner failure may not find its way into the statistical data or, conversely, a non-failed burner may be replaced because it is convenient or cheaper to do so at that time.

The burner failure mechanism is further complicated by the complex nature of the failures. There is seldom a single cause. By the time a failed burner is examined, the basic causes of failure may be obscured by secondary failures.

2.2.2 Selection of Failure Modes

Because of the difficulties in obtaining representative failure data outlined above, P&WA instituted an airline burner survey. The condition of a fixed number of JT9D-7 burners at engine removal was noted in detail. The cause of engine removal need not have been the burner. A representative sampling of airlines was used to include a range of tough (full power, hot climate) to easy (de-rated, cold climate) operators. Burner data was obtained for burners with up to 8000 hours of operation.

Although the condition of the burners observed in the survey varied greatly, depending on the operator and the number of cycles and hours, the location of cracks was consistent. Figure 18 is a plot of the frequency of cracks in the inner liner for 5 of the burners reported in the survey. In Table 1 the results of the survey for one operator are summarized. While the number of cracks increases with cycles and hours, other forms of distress are random. Metal erosion is the least frequent form of distress and in most cases it is related to louver lip buckling or some other damage immediately upstream of the erosion.

In addition to the special survey data, in-house testing and field service testing data for the JT9D-7 and TF30 P-100 and P-412A engines was reviewed to define the primary failure modes.

The failure modes selected are lip buckling and creep-low cycle fatigue (LCF) interaction (cracking). A third failure mode, oxidation/erosion, was considered to be a secondary failure mode, as erosion damage seen on burners is generally the result of louver lip collapse.

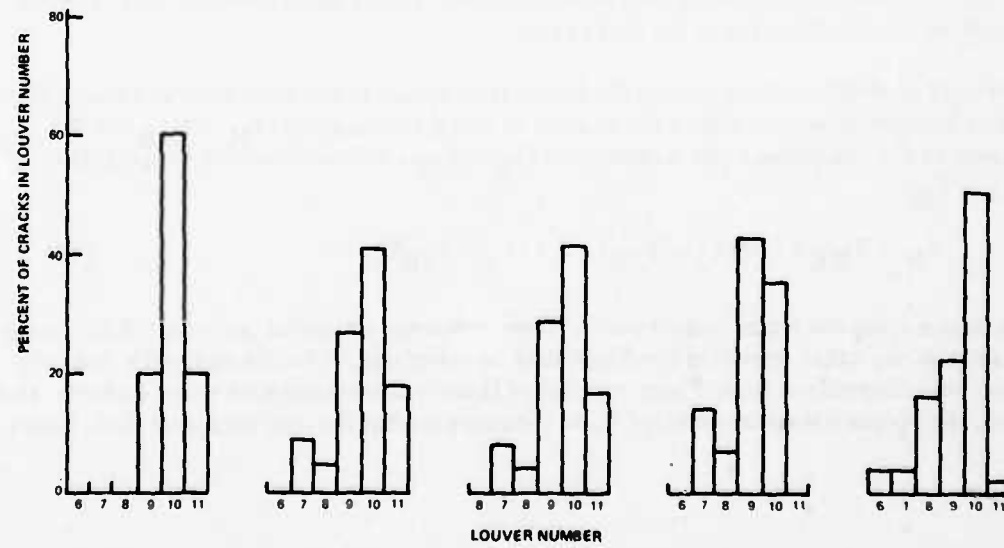


Figure 18 Axial Crack Frequency Study

TABLE I
RESULTS OF AIRLINE BURNER SURVEY FOR JT9D-7 SINGLE OPERATOR

Hours	1268	3421	3783	4058	4136
Cycles	801	2238	2256	2385	2476
ID Damage (No. of Locations)					
Axial Cracks	9	12	27	43	43
Circumferential Cracks	—	9	—	5	1
Louver Creep and/or Buckling	—	12	—	21	1
Metal Erosion and/or Burn Through	—	5	—	—	—
OD Damage					
Axial Cracks	9	18	67	65	27
Circumferential Cracks	—	2	—	4	—
Louver Creep and/or Buckling	13	10	—	—	—
Metal Erosion and/or Burn Through	3	1	—	—	—

2.2.3 Description of Burner Failure Modeling

2.2.3.1 Temperature Simulation

The calculation of burner life due to LCF-creep interaction cracking and louver lip buckling requires knowing the burner temperatures and using these temperatures to predict the resultant stresses and strains. Since the model will not include complete thermal or stress analysis, temperatures and strain ranges will be input along with the compressor exit and turbine inlet temperature for a reference condition. The program will then vary temperatures and stresses throughout the flight cycle.

For the hot metal temperatures of the louver (this occurs at the weld joint and louver lip) the following expression relates the changes in metal temperature ($T_M - T_{MR}$) to the change in the compressor exit temperature ($T_3 - T_{3R}$) and turbine inlet temperature ($T_4 - T_{4R}$):

$$T_M - T_{MR} = 0.6 (T_3 - T_{3R}) + 0.4 (T_4 - T_{4R}) \quad (18)$$

By determining the metal temperature at some reference condition (subscript R) the temperature at any other operating condition may be calculated. The constants (0.6 and 0.4) have been determined from a large number of thermocouple tests with many burners. However, the program is set up to input these constants so that the user may alter these values.

To complete the structural analysis, a temperature gradient between the hot portion of the louver (T_M) and the cold portion shielded by the lip (T_K) must be known. This temperature is related to the compressor exit temperature (T_3) by:

$$T_K = T_3 + 20^\circ F \quad (19)$$

This expression is simpler than the expression given in the first interim report for this contract (Ref. 1) while providing essentially the same values.

2.2.3.2 Elastic-Plastic Analysis

Air-cooled combustion chamber liners experience large, thermally-induced strains that exceed the elastic limits of the material at points of maximum stress and/or temperature. As illustrated in the typical stress-strain-temperature curve of Figure 19, once the proportional limit has been exceeded, the simple proportional relationship between stress and strain is lost and the problem becomes considerably more difficult.

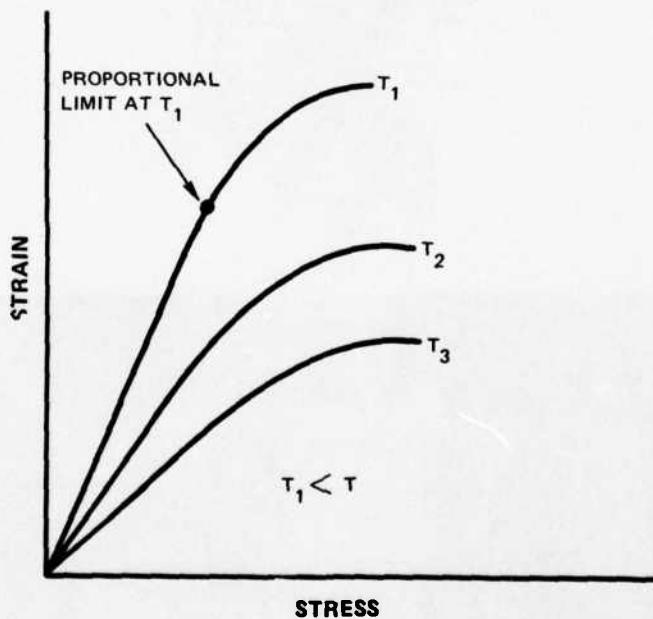


Figure 19 Typical Stress-Strain-Temperature Relationship

Analytical procedures which handle both elastic and plastic conditions are only now becoming available. To make use of these programs would require combining an entire structural analysis program with the mission analysis program and failure model. As noted before, that is beyond the scope of this work. Therefore a portion of the analysis for both creep-LCF and louver lip buckling involves developing procedures for adapting the elastic analysis to a plastic situation.

2.2.3.3 Creep-Low Cycle Fatigue Failure Model

Examples of typical combustion chamber liner failures are illustrated in Figures 20 and 21. The cracking shown in Figure 20 is characteristic of LCF failures in can-annular combustion chambers. Cracking initiates in the region of the seam welding joggle radius and progresses circumferentially around the liner. The liner must be removed and repaired to prevent separation when such cracks are found in hot-section inspection. Figure 21 illustrates the typical cracking failure mode experienced in large diameter annular combustion liners. In this case, cracking initiates either at the louver lip edge or sometimes in the seam weld and then progresses axially. As in the case of the can-annular liner, the burner must be removed and repaired before the axial crack reaches a critical length which, fortunately, can be in the order of several inches.

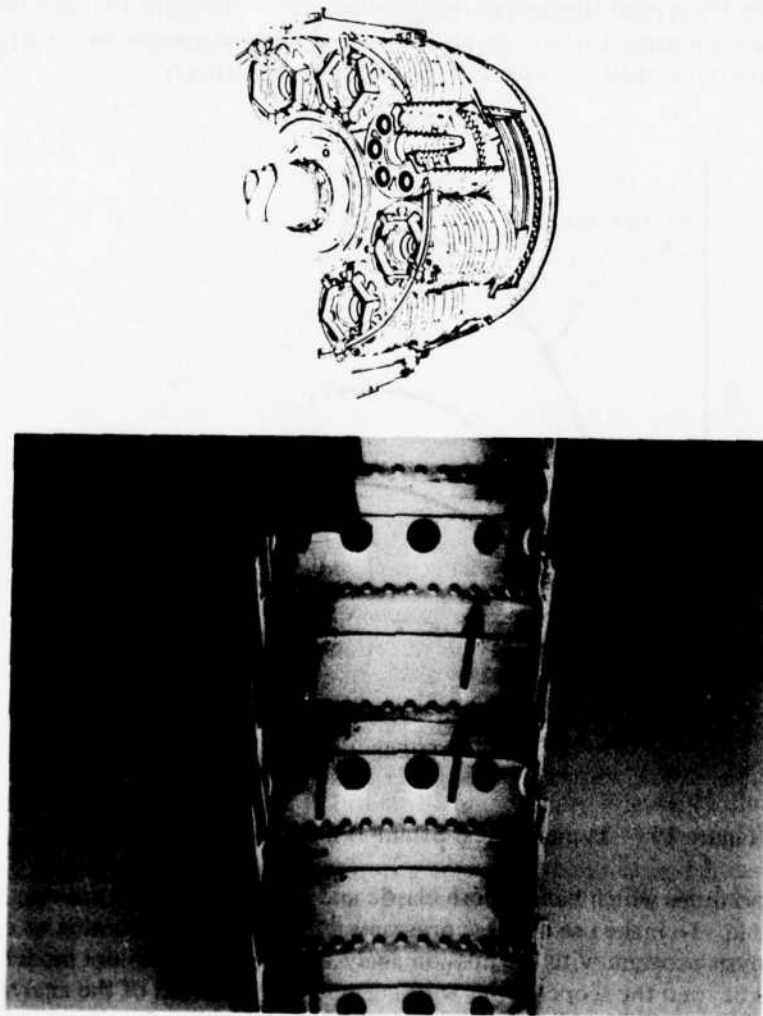


Figure 20 Typical Circumferential Cracks in Can-Annular Burner

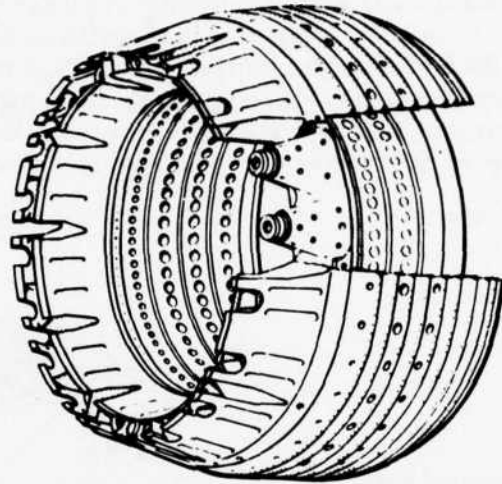


Figure 21 Typical Axial Cracks in an Annular Liner

Both of the cracking modes described above are caused by cycling of the thermal gradient between the hot louver lip and the cold louver knuckle. This gradient results in a high hoop stress in the lip-seam weld area and a high bending stress in the seam weld-joggle radius area. The relative magnitudes of these bending and hoop stresses are dependent upon the liner radius. Smaller radius liners (can-annular burners) have bending stresses higher than hoop stresses and hence failure is by circumferential cracking. Large radius liners (annular burners) have hoop stresses higher than bending stresses and hence failure is by axial cracking. The relative magnitudes of hoop and bending stress components as a function of liner radius are given in Figure 22.

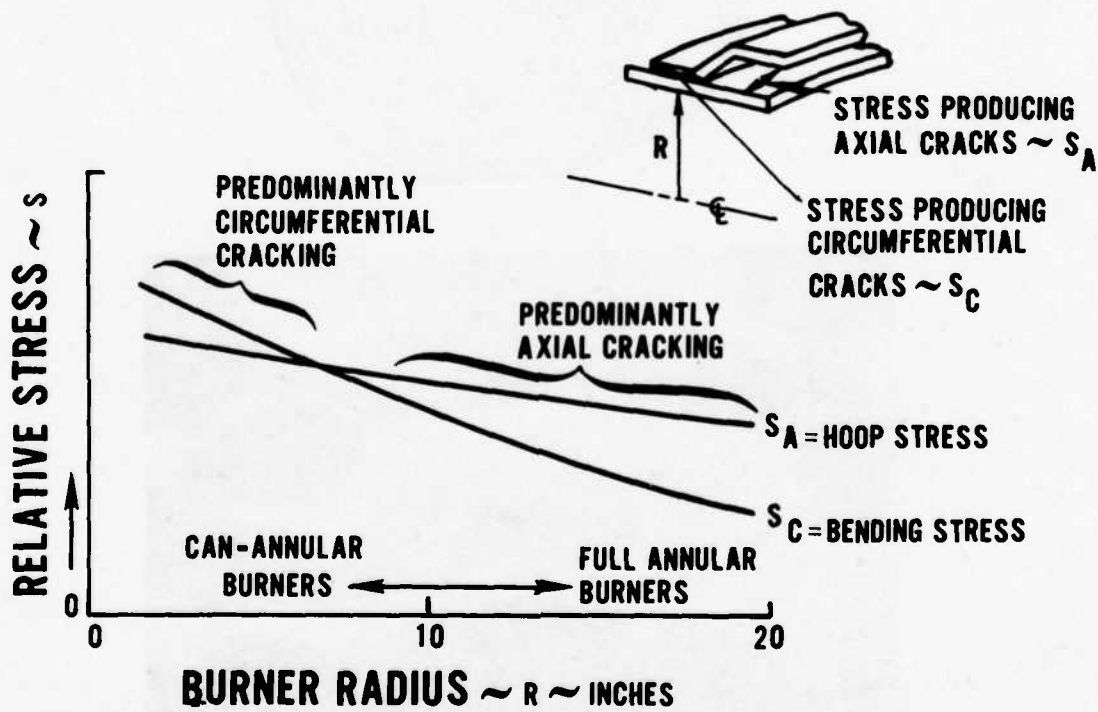


Figure 22 Relative Magnitude of Hoop and Bending Stress Components vs. Liner Radius

2.2.3.3.1 Damage Model Formulation

For a typical flight cycle, a hysteresis loop similar to that of Figure 23 can be used to represent stress-strain relationships. The portion of the curve from the origin to point A represents stress-strain at transient conditions from idle to takeoff. The dwell, representing time at SLTO, climb and cruise is depicted by the constant strain portion of the curve, A-B. Descent is represented by the remainder of the cycle, B-C.

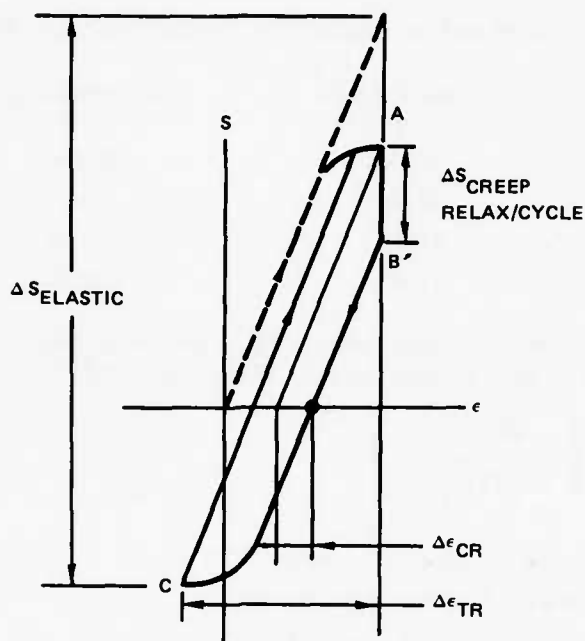


Figure 23 Typical Stress-Strain Hysteresis Loop

In order to break up the problem into tractable components, the inelastic strains occurring within the cycle are segregated into a time-independent (plastic) strain component and a time-dependent creep strain component according to the concept proposed by S. S. Manson (Ref. 3). The time-independent plastic strain range component is that which would occur if the reversal took place immediately without any dwell at the maximum strain condition. The time-dependent strain component is taken as the additional inelastic strain which occurs as a result of the dwell at maximum strain.

Manson defines four combinations of creep and plasticity that can be used as building blocks for partitioning complex cycles:

$\Delta \epsilon_{pp}$ – tensile plastic strain reversed by compressive plastic strain

$\Delta \epsilon_{pc}$ – tensile creep strain reversed by compressive plastic strain

$\Delta \epsilon_{cp}$ – tensile plastic strain reversed by compressive creep strain

$\Delta \epsilon_{cc}$ – tensile creep strain reversed by compressive creep strain

These four definitions can be summarized in the following table taken from Reference 2:

<u>Notation</u>	<u>Tensile Strain</u>	<u>Compressive Strain</u>
$\Delta\epsilon_{pp}$	plastic	plastic
$\Delta\epsilon_{pc}$	plastic	creep
$\Delta\epsilon_{cp}$	creep	plastic
$\Delta\epsilon_{cc}$	creep	creep

The time-independent reversed plastic strain is $\Delta\epsilon_{pp}$ (no creep component), and the damage associated with it, is given by an expression of the form [Ref. 3]:

$$\frac{1}{N_{pp}} = \left(\frac{\Delta\epsilon_{pp}}{0.75 D_p} \right)^{1/a} \quad (20)$$

where: a is a constant related to the material
 D_p is the tensile ductility of the material
 N_{pp} is the number of cycles to cracking

The damage associated with the time-dependent creep strain components depends on the predominant cracking mode. In the case where the hoop stress, and consequently the axial mode of cracking, is dominant, the creep damage component is of the $\Delta\epsilon_{pc}$ type.

The combustor lip, as it heats up, cannot grow because of the restraint of the cold knuckle and is therefore in compression, and, at the high temperatures, the damage mechanism is creep. When the cycle is reversed and the lip is cold, the tensile strain is plastic. The damage is then given by [Ref. 3]:

$$\frac{1}{N_{pc}} = \left(\frac{\Delta\epsilon_{pc}}{1.25 D_p} \right)^{1/b} \quad (21)$$

where: b is a constant related to the material
 N_{pc} is the number of cycles to cracking

If the bending stress, and therefore circumferential cracking mode, is dominant, then both the $\Delta\epsilon_{cp}$ and $\Delta\epsilon_{pc}$ type strains are present. On the surface that is in tension when the material is hot, the mechanism is $\Delta\epsilon_{cp}$ (tensile creep strain reversed by compression plastic strain), while on the opposite surface the mechanism is one of compressive creep reversed by plastic strain. Observations that combustor cracks were initiated on the side in tension at high temperature confirmed Manson's conclusion that the $\Delta\epsilon_{cp}$ was more damaging than the $\Delta\epsilon_{pc}$ cycle. However, damage was best correlated with the expression for N_{pc} , (Equation 21) rather than that proposed by Manson for N_{cp} :

$$\frac{1}{N_{cp}} = \left(-\frac{\Delta \epsilon_{cp}}{0.25 D_c} \right)^{1/b} \quad (22)$$

where: D_c is the creep ductility

The two forms of damage are assumed to be linearly accumulative, leading to the total life:

$$\frac{1}{N_t} = \frac{1}{N_{pp}} + \frac{1}{N_{pc}} \quad (23)$$

2.2.3.3.2 Determination of Time-Independent Plastic Strain Range, $\Delta \epsilon_{pp}$

As noted earlier, the calculation of cyclic plastic strains and strain ranges is a difficult analytical task. Instead, the total strain range, $\Delta \epsilon_{tr}$, is approximated from the elastic stress: (See Figure 23)

$$\Delta \epsilon_{tr} = \Delta \epsilon_{elastic}/E \quad (24)$$

The LCF strength of materials is commonly specified in curves showing the cycles to cracking as a function of the total strain range (elastic and plastic) on a log scale. These curves have the form shown in Figure 24, and several models have been proposed in the literature to relate the LCF curves to common material properties. The model proposed by Langer [Ref. 4] envisions the curve to be found by the sum of the elastic, $\Delta \epsilon_e$, and plastic, $\Delta \epsilon_{pp}$, strain range components. Using this model, the plastic strain range can be determined by subtracting elastic strain from the total strain range:

$$\Delta \epsilon_{pp} = \Delta \epsilon_{tr} - \Delta \epsilon_e \quad (25)$$

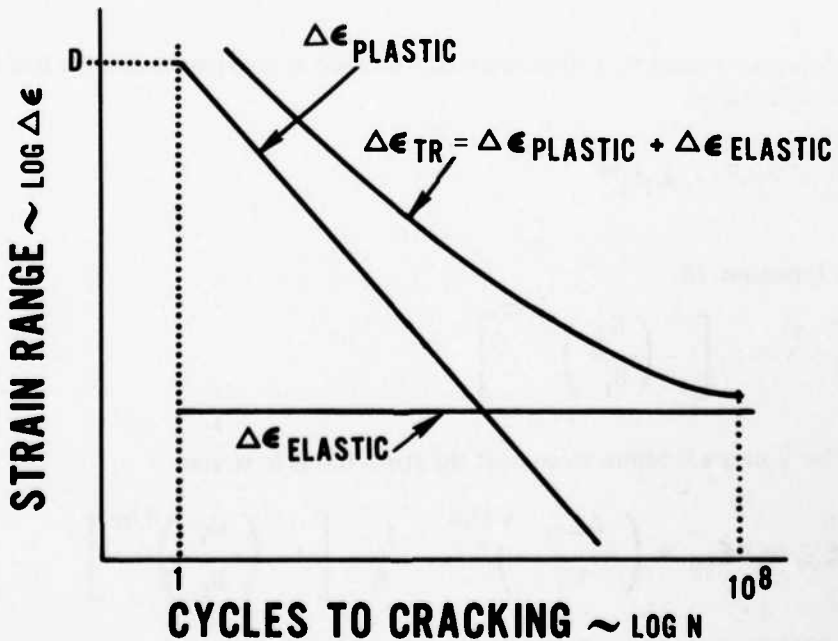


Figure 24 Typical LCF Life-Strain Log Plot with Langer's Hypothesis

Equation 25 provides a simple estimate of plastic strain range, requiring only the total strain range as calculated by elastic analysis and the value $\Delta \epsilon_e$ as estimated from the conventional endurance limit or curve fit for actual LCF data.

2.2.3.3.3 Determination of Time-Dependent Strain Range, $\Delta \epsilon_{pc}$ or $\Delta \epsilon_{cp}$

In general the stresses/strains causing failure in combustor liners are the direct result of thermal growth incompatibilities and, as such, come under the class of strain-controlled cyclic problems. It is postulated that the creep strains induced during a typical cycle are primarily the result of stress relaxation at constant total strain. Referring to Figure 23, the creep strain associated with a given stress relaxation is taken as the change in elastic strain, or simply as $\Delta S_{creep}/E$.

In order to obtain a closed-form solution for the stress relaxation occurring in a cycle, a relationship between creep, stress and time proposed by J. Marin [Ref. 5] is assumed:

$$\epsilon = [K_1 + K_2(1 - e^{-qt}) + K_3t] S^m \quad (26)$$

The first term in the brackets in Equation 26 is proportional to the initial loading strain, the second term is proportional to the transient creep strain, and the third term is proportional to the steady-state creep strain.

Since, for a given material, the expression within the brackets is only a function of temperature, Equation 26 can be simplified to:

$$\epsilon = B_t S^m \quad (27)$$

Since the process is assumed to be one of stress relaxation at constant strain, the strain must remain at its initial value:

$$\epsilon_i = B_t S^m = K_1 S_i^m \quad (28)$$

Rearranging Equation 28.

$$S_i - S = S_i \left[1 - \left(\frac{K_1}{B_t} \right)^{1/m} \right] \quad (29)$$

and dividing by Young's Modulus to convert the stress terms to strains:

$$\Delta \epsilon_{pc} \text{ or } \Delta \epsilon_{cp} = \left(\frac{\Delta \epsilon_{tr}}{K_1} \right)^{1/m} - \frac{1}{E} \left[1 - \left(\frac{K_1}{B_t} \right)^{1/m} \right] \quad (30)$$

In Equation 30 the initial strain, ϵ_i , has been replaced by its equivalent, the total strain range as calculated by elastic analysis.

2.2.3.3.4 Determination of K_1 , m and B_t

One way the stress (S)-strain (ϵ) relationship of a metal can be represented mathematically is:

$$\epsilon = S/E \text{ for } S < S_{pl} \quad (31a)$$

$$\epsilon = aS^b + S/E \text{ for } S \geq S_{pl} \quad (31b)$$

where: a, b are constants for a given material

E is Young's Modulus

S_{pl} is the proportional limit of the material

Since the combustor sustains damage at conditions beyond the proportional limit, the stress-strain relationship can be represented, with little loss in accuracy as:

$$\epsilon = aS^b \quad (32)$$

Rewriting Equation (26) for the non-time-dependent situation:

$$\epsilon = K_1 S^m \quad (33)$$

Therefore, K_1 and m are constant for a given material, and their values can be determined by a logarithmic plot of the stress-strain relationship in the plastic range (see Figure 25).

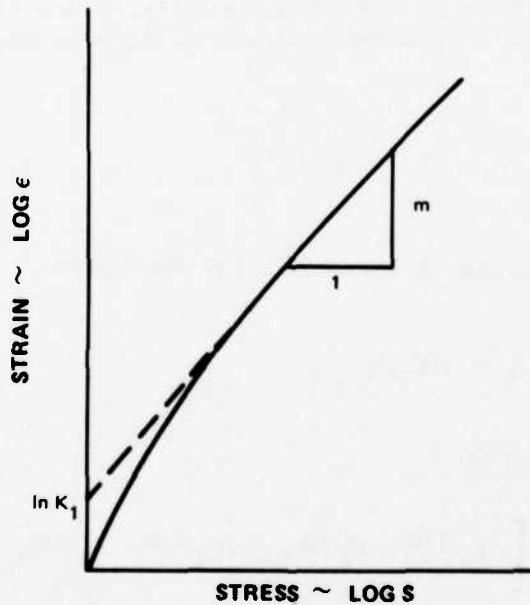


Figure 25 Typical Log Plot of Stress-Strain Relationship in the Plastic Region

B_t can be considered as analogous to K_1 . Unlike K_1 , however, B_t is both time and temperature dependent and requires creep data for its determination.

In materials manuals, creep data is represented by a series of stress-time curves for various temperatures (Figure 26a). Each curve represents a different percent creep for the material. The format is cumbersome, and numerous procedures have been proposed to condense creep and rupture data to a single set of curves. Larson-Miller [Ref. 6] proposed the parameter $(T + 460)(C + \log t)$, where T is the temperature in °F, t the time in hours, and C a material-dependent constant (Figure 26b). For most materials, C ranges between 14 and 22, with 20 a good average number if specific data is missing [Ref. 7].

For a given flight interval, time and temperature are determined and used to enter a Larson-Miller-type creep plot. The intercepts of the constant-creep lines define a stress-strain curve for the material at the time and temperature of the flight interval (Figure 26c). In an analogous plot to that used to determine K_1 , B_t is the intercept of the logarithmic stress-strain plot.

2.2.3.3.5 Creep/Relaxation Under Various Hold Conditions

A typical aircraft mission cycle involves hold periods at various power conditions, and, therefore, at various temperature levels. In order to employ Equation 17 at the different temperature levels and accumulate the creep damage, a Time Hardening Theory [Ref. 8] has been adopted.

The concept of the Time Hardening Theory is illustrated graphically in Figure 27. The first hold condition occurs at temperature T_1 for a time period t_1 . At time = t_1 conditions change, and the liner is at temperature T_2 until time is equal to t_2 . Equation 30 can be rewritten in the form:

$$\Delta\epsilon_{cr} = \frac{A}{E} \left[K_1^{-1/m} - B_t^{-1/m} \right] \quad (34)$$

To calculate the creep strain $(\Delta\epsilon_{cr})_i$ that occurs in any time interval:

$$\Delta\epsilon_{cr,i} = \Delta\epsilon_{cr,t_i} - \Delta\epsilon_{cr,t_{i-1}} \quad (35)$$

Combining equations 34 and 35:

$$\Delta\epsilon_{cr,i} = \frac{A}{E} \left[(K_1^{-1/m} - B_t^{-1/m})_{t_i} - (K_1^{-1/m} - B_t^{-1/m})_{t_{i-1}} \right] \quad (36)$$

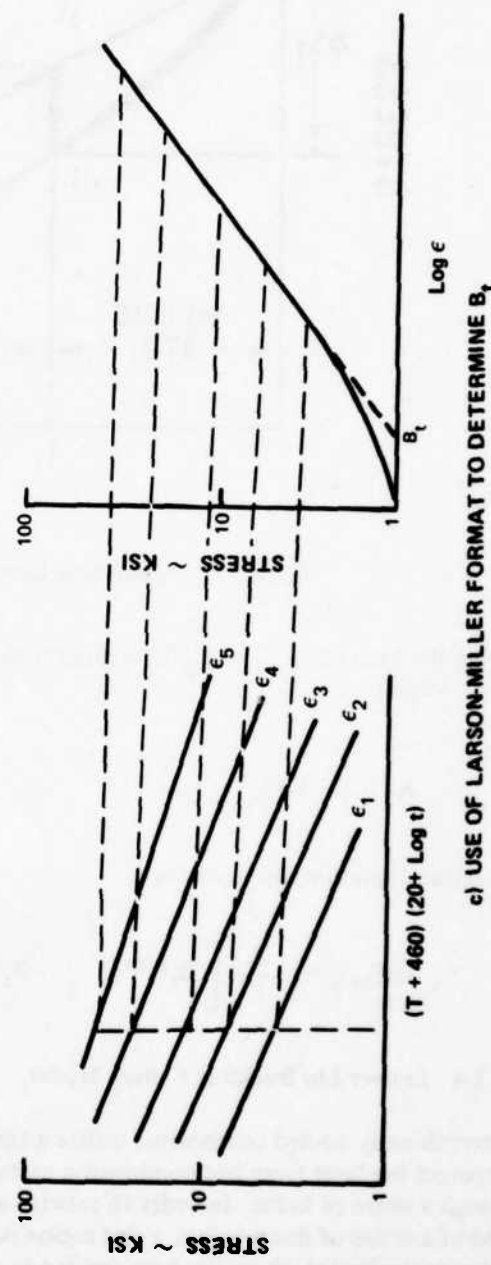
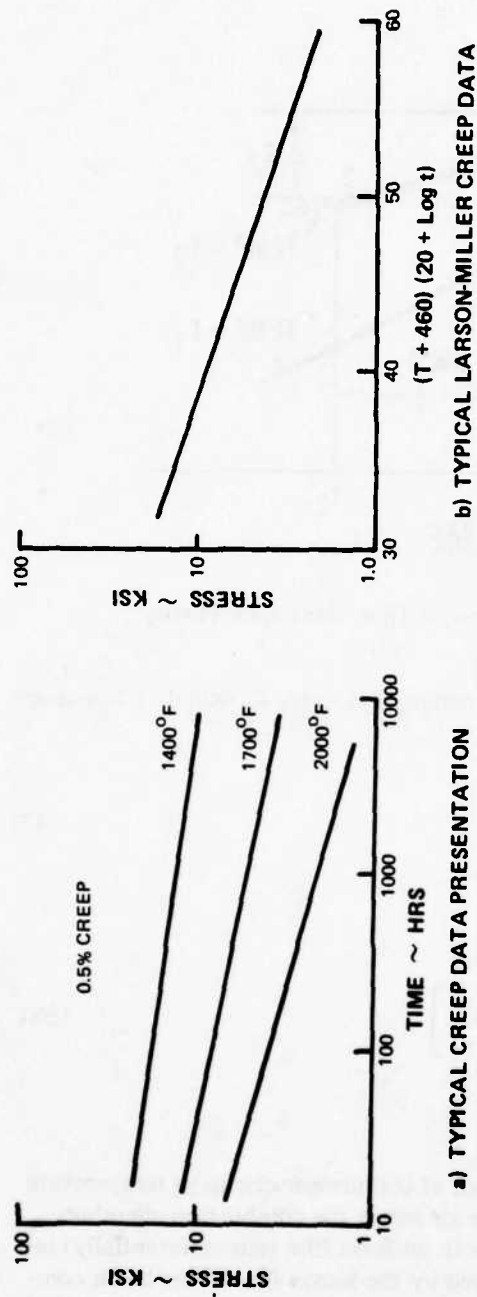


Figure 26 Creep Data – B_t Relationship

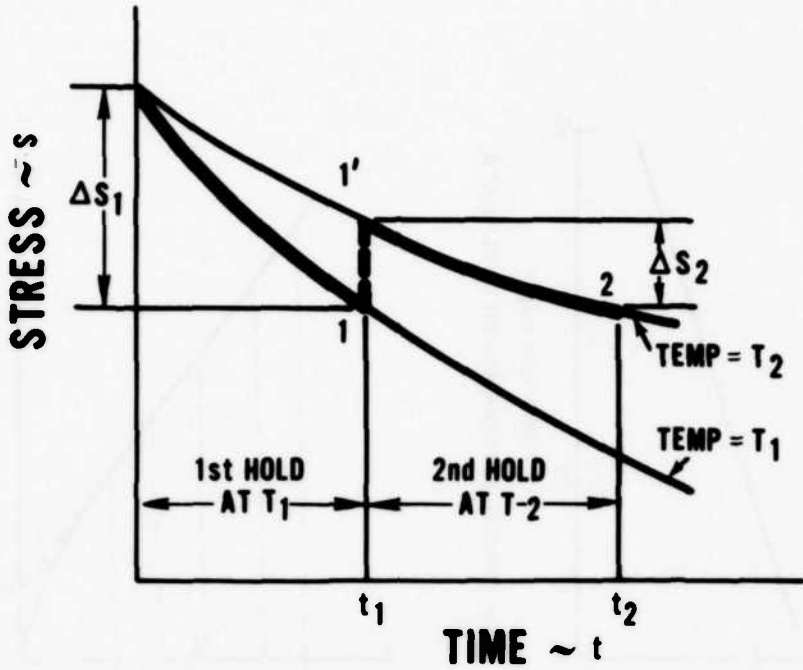


Figure 27 Graphical Description of Time-Hardening Theory

During the interval t_{i-1} to t_i , the temperature is constant, and, since K_1 is only a function of temperature:

$$K_1)_{t_i} = K_1)_{t_{i-1}} \quad (37)$$

Therefore Equation 36 becomes:

$$\Delta \epsilon_{cr})_i = \frac{A}{E} \left[B_t^{-1/m})_{t_{i-1}} - B_t^{-1/m})_{t_i} \right] \quad (38)$$

2.2.3.4 Louver-Lip Buckling Failure Model

Conventionally cooled combustors utilize a film of air at compressor discharge temperature to protect the liner from hot combustion gases. The air enters the combustion chambers through a series of holes. In order to provide a smooth uniform film (circumferentially) instead of a series of discrete jets, a slot region is formed by the louver lip. In the harsh combustor environment, these lips have tended to collapse in just those regions of the liner that were hottest, in-line with fuel nozzles, for example. This led to a cutting off of the cooling flow where it was most urgently needed, resulting in burning of the metal and progressive deterioration further downstream.

To reduce the metal temperature of the combustor, coatings were added to the hot side of the liner to act as an insulating barrier. While the reduction in metal temperature was not great in absolute numbers, it was frequently sufficient to bring the combustor under a threshold level above which deterioration was very rapid. One shortcoming of the earlier coatings was their tendency to flake off or erode. Efforts to improve the adherence of the coating were successful.

When louver-lip buckling was identified as a major combustor failure mechanism, early modeling attempts utilized a bi-metallic strip theory: as the coating heats up more than the metal, it expands and, adhering to the metal, curls the lip inward, thus causing buckling. Several laboratory tests altered this theory. The coating did indeed expand more than the metal, but the cause of the expansion was a phase change in the coating brought about by oxidation.

Two distinct phenomena cause louver-lip buckling. One is the aforementioned coating expansion effect, and the other is thermal buckling caused by the thermal growth of the lip as it heats up. Restrained by the cold knuckle, the lip relieves itself by buckling. (See Figure 28) The amount of louver-lip buckling is:

$$W = W_b + \sum_i W_{ci} \quad (39)$$

where: W_b is the amount of thermal buckling that occurs at the worst flight condition. This is a one time occurrence.

W_{ci} is the amount of coating-induced buckling at flight condition. It is cumulative, but the rate varies, depending on whether thermal buckling has occurred or not.

Failure is assumed to occur when the lip closes completely.

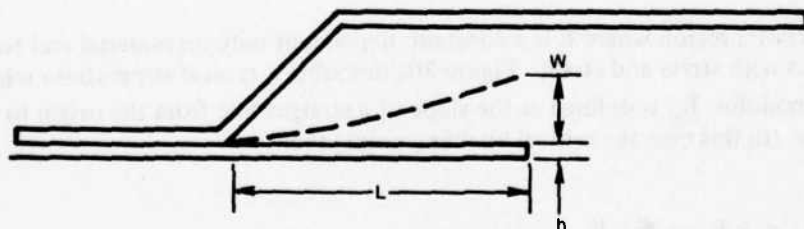


Figure 28 Combustor Louver-Lip Buckling Nomenclature

2.2.3.4.1 Thermal-Buckling Model

The tendency of the louver lip to buckle is a result of the temperature difference between the hot-lip and the cold-knuckle regions of the louver. An elastic-plastic model for louver-lip buckling has been developed with a critical lip-buckling temperature determined as a function of the geometry and lip-knuckle gradient.

A lip buckling coefficient k is defined as:

$$k = S_{ce}/E \quad (40)$$

where: E is Young's Modulus

S_{ce} is the elastic buckling stress

Figure 29 relates the buckling coefficient, k , to the geometry of the louver (radius, lip length, and thickness). The value of k which is independent of both material and temperature, was determined by a parametric analysis of shells.

As was noted in the creep/LCF section, at the stresses and temperatures of interest the combustor material is beyond its elastic limit, reducing the usefulness of Equation 40. The assumption is made that Equation 40 can be written:

$$k = S_c/E_t \quad (41)$$

where: E_t is the slope of the material stress-strain curve in the plastic region, called the tangent modulus.

S_c is the critical buckling stress.

Unlike the elastic region where E is a constant, dependent only on material and temperature, E_t also varies with stress and strain. Figure 30a describes a typical stress-strain relationship. If a secant modulus, E_s , is defined as the slope of a straight line from the origin to any point on the curve, (in this case the critical buckling point) then:

$$S_c = k E_t = \epsilon_c E_s \quad (42)$$

or

$$\epsilon_c/k = E_t/E_s)_{cr} \quad (43)$$

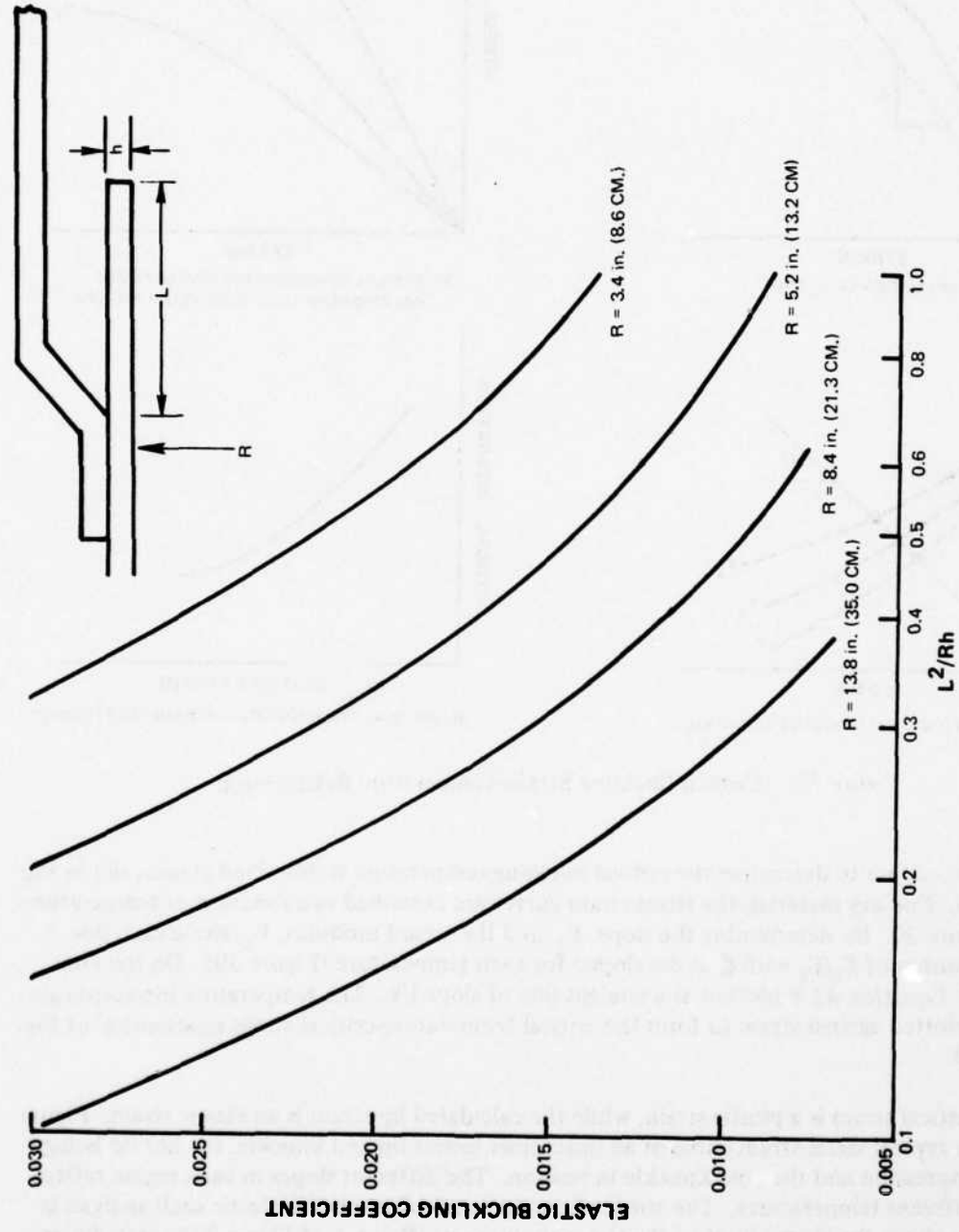


Figure 29 Elastic Buckling Geometry Relationship

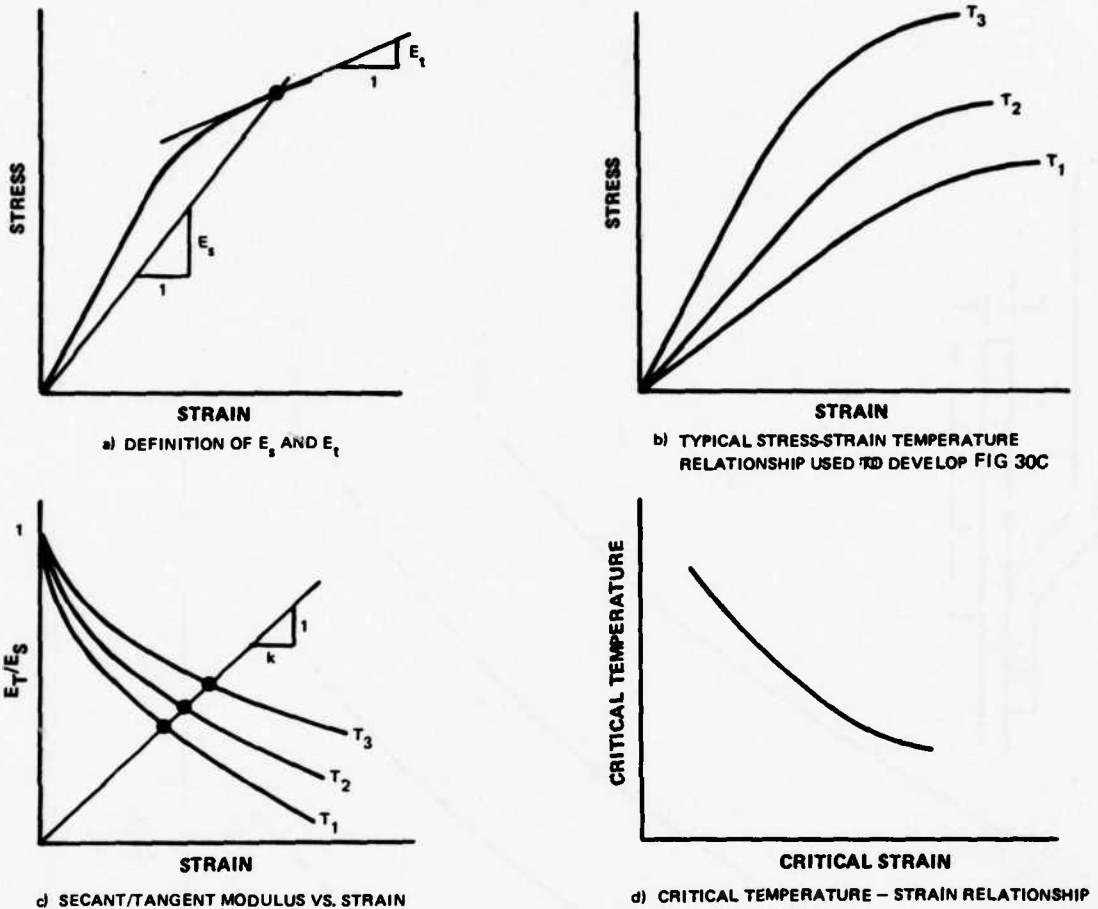


Figure 30 Critical Buckling Strain-Temperature Relationship

The procedure to determine the critical buckling temperature is described graphically in Figure 30. For any material, the stress-strain curves are described as a function of temperature in Figure 30. By determining the slope, E_t , and the secant modulus, E_s , along each line, a relationship of E_t/E_s with ϵ is developed for each temperature (Figure 30). On the same figure, Equation 42 is plotted as a straight line of slope $1/k$. The temperature intercepts are then plotted against strain to form the critical temperature-critical strain relationship of Figure 30.

The critical strain is a plastic strain, while the calculated lip strain is an elastic strain. Figure 31 is a typical stress-strain curve of an outer liner louver lip and knuckle, the hot lip being in compression and the cold knuckle in tension. The different slopes in each region reflect the different temperatures. The stress of the lip as calculated by an elastic shell analysis is clearly above the elastic limit of the stress-strain curve (Point A of Figure 31), while Point A' represents the stress-strain conditions of the cold, unyielded knuckle.

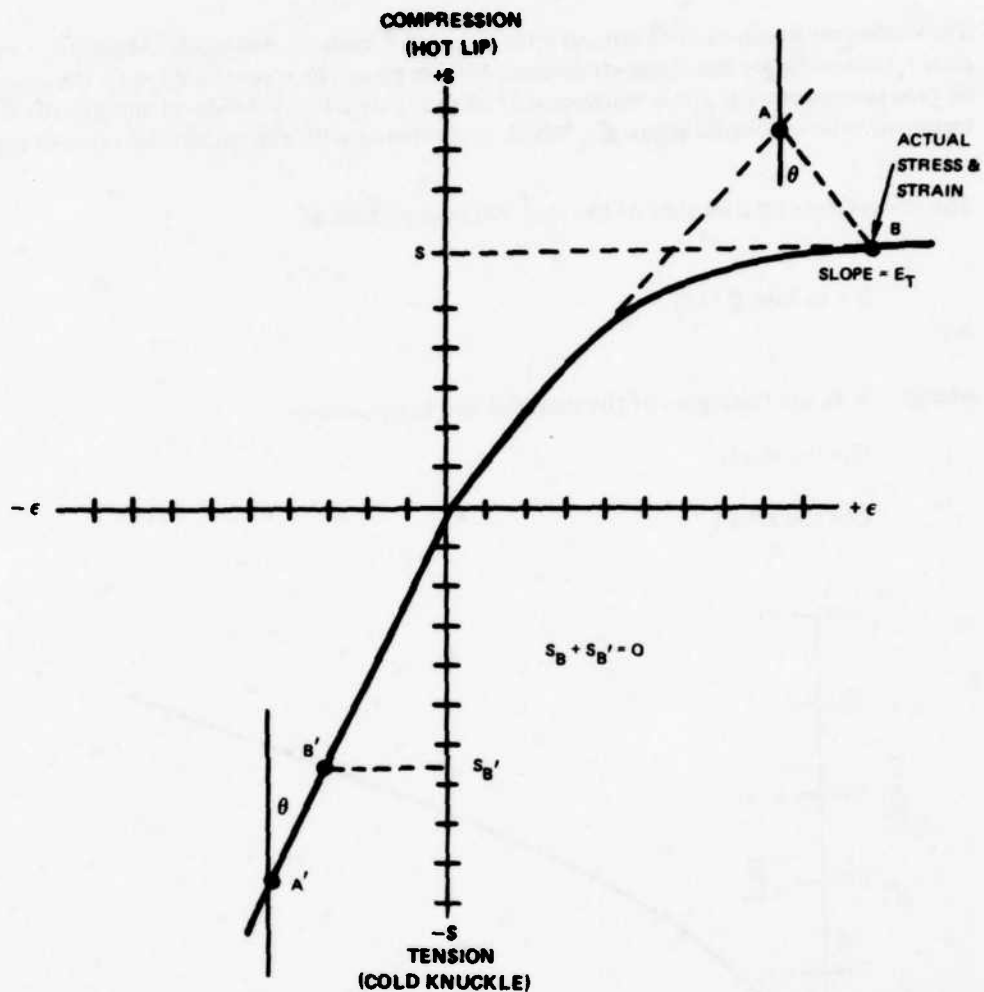


Figure 31 Typical Stress-Strain Curve For Lip Buckling Model

The approach to the plasticity problem follows from the fact that the sum of the thermal loads (stresses) on the shell structure must equal zero, while the strain is assumed to be equal to that predicted by the elastic analysis. Since the actual stresses must lie upon the stress-strain curve (See Figure 31), a new equilibrium condition (B-B') must exist. If that strain exceeds the strain required to cause buckling, then the amount of thermal buckling is determined from a curve of strain vs. amplitude (Figure 32). This curve is independent of materials and radius. It relates the loading on the hoop to the deflection required to relieve the load. The number of waves varies with radius but the wave length is independent of radius, thus making Figure 33 general for all materials and geometry. The value of thermal deflection is taken as the maximum value seen throughout the life cycle.

The computer program does not perform the above analysis graphically. Instead, a mathematical relationship for the stress-strain-temperature property is combined with the assumptions of zero stress-constant strain range described in Figure 31 to provide an analytically determined value of elastic strain ϵ_A which is compared with the calculated value of lip strain.

The stress-strain relationship of the material is expressed as:

$$S = m \log \epsilon + b \quad (44)$$

where: b , m are functions of the material and temperature

S is the stress

ϵ is the strain

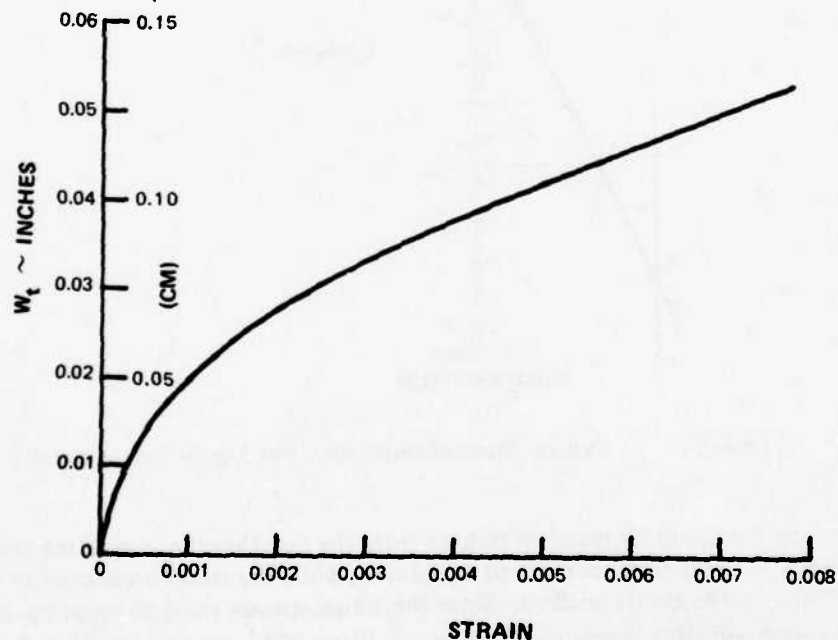


Figure 32 Thermal Buckling Deflection vs. Lip Strain

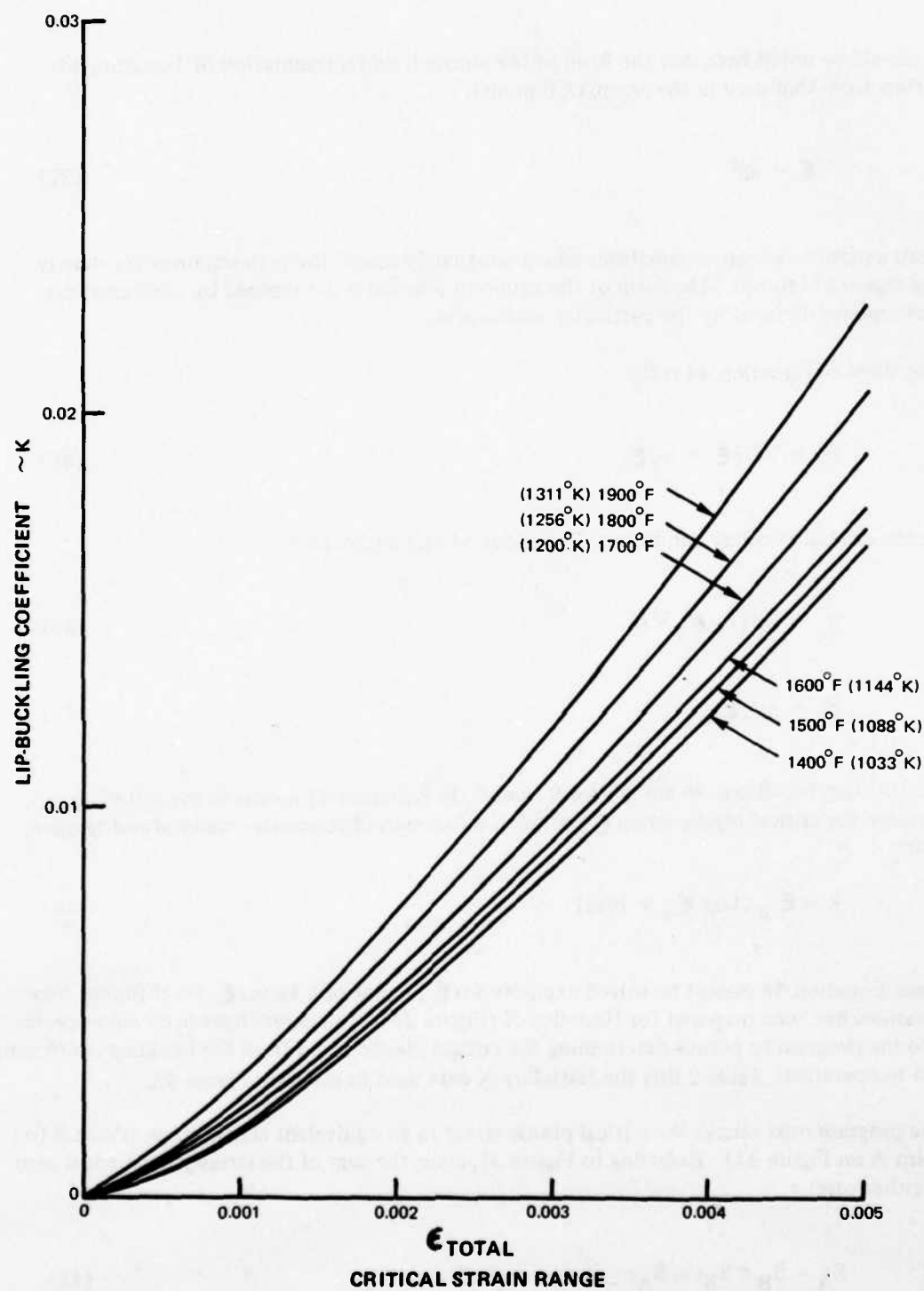


Figure 33 Critical Strain Range – Buckling Coefficient Relationship

It should be noted here that the form of the stress-strain representation of Equation 44 differs from that used in the creep/LCF model:

$$\epsilon = aS^b \quad (32)$$

Both equations are approximations which adequately model the material property data in the region of interest. The form of the equation selected is determined by mathematical convenience dictated by the particular application.

The slope of Equation 44 is E_t :

$$E_t = \partial S / \partial \epsilon = m / \epsilon \quad (45)$$

At the critical buckling conditions, Equations 44 and 45 become:

$$S_c = m / \log \epsilon_c + b \quad (46)$$

$$E_t = m / \epsilon_c \quad (47)$$

Substituting Equations 46 and 47 for S_c and E_t in Equation 41 results in the following expression for critical plastic strain ϵ_c which is a function of geometry, material and temperature.

$$k = \epsilon_c [\log \epsilon_c + b/m] \quad (48)$$

Since Equation 48 cannot be solved explicitly for ϵ_c , a plot of k versus ϵ_c for different temperatures has been prepared for Hastelloy-X (Figure 33). The curves have been incorporated into the program to permit determining the critical plastic strain from the buckling coefficient and temperature. Table 2 lists the Hastelloy-X data used to generate Figure 33.

The program next relates the critical plastic strain to an equivalent elastic strain (Point B to Point A on Figure 31). Referring to Figure 31, since the sum of the stresses must equal zero in either case:

$$S_A - S_B = S_{B'} - S_{A'} \quad (49)$$

TABLE 2
HASTELLOY-X PROPERTIES USED TO CALCULATE THERMAL BUCKLING

TEMP. °F	m		b		E x 10 ⁻⁶	
	(°K)	psi (MPa)	psi (MPa)	psi (MPa)	psi (MPa)	E x 10 ⁻⁶ (MPa)
1000	811	11813	81.4	102019	703.4	24.6
1400	1033	10431	71.9	90151	621.6	22
1500	1088	9427	65.0	82117	566.2	21
1600	1144	7781	53.6	68837	474.6	19.9
1700	1200	5597	38.6	51074	352.1	18.5
1800	1256	3650	25.2	34478	237.7	17
1900	1311	2166	14.9	21371	147.4	15.5
						0.107

To maintain a constant strain:

$$\epsilon_B - \epsilon_A = \epsilon_{B'} - \epsilon_{A'} \quad (50)$$

Dividing Equation 49 by 50.

$$\frac{S_A - S_B}{\epsilon_B - \epsilon_A} = \frac{S_{B'} - S_{A'}}{\epsilon_{B'} - \epsilon_{A'}} \quad (51)$$

Since the cold knuckle is in the elastic range, $(S_{B'} - S_{A'}) / (\epsilon_{B'} - \epsilon_{A'})$ represents Young's Modulus of the knuckle material:

$$\frac{S_A - S_B}{\epsilon_B - \epsilon_A} = E' \quad (52)$$

For the hot lip, the following stress-strain relationships apply in the elastic and plastic regions respectively:

$$S_A = \epsilon_A E \quad (53)$$

$$S_B = \ln \epsilon_B + b \quad (54)$$

Combining equations 52, 53, and 54, and solving for ϵ_A :

$$\epsilon_A = \frac{\epsilon_B E' + \ln \epsilon_B + b}{E + E'} \quad (55)$$

If the strain at Point B represents the critical plastic strain then ϵ_A is the equivalent elastic strain that will cause the lip to buckle.

To summarize the procedure for determination of the equivalent elastic strain at which buckling will occur:

- 1) A buckling coefficient based only upon geometry is determined (Figure 29).
- 2) A plastic buckling strain is determined from Equation 48 or Figure 33.
- 3) An equivalent elastic strain is determined, based upon the assumptions that the sum of the stresses are zero while the total strains are equal in either the actual plastic case or the calculated elastic case (Equation 55).

2.2.3.4.2 Coating-Induced Buckling

Oven tests of magnesium-zirconate coated Hastelloy-X strips confirmed the oxidation-volume change bimetallic strip mechanism of louver-lip deflection. This data, presented in the form of curves (Figure 34) of strip deflection vs. time-at-temperature forms the basis of the coating-induced buckling model.

The extent of coating-induced buckling during a flight increment is:

$$w_{ci} = C_{ri} \left(\frac{L}{1.5} \right)^2 \delta_i \quad (56)$$

where C_r is a hoop restraint factor

L is the louver lip length

δ_i is the strip deflection that results from time t_i at temperature T_i

The hoop restraint factor, depending on the geometry, temperature, and whether the lip has buckled thermally at some prior flight point, is determined from Equation 57a (thermally buckled) or 57b (thermally unbuckled):

$$C_{ri} = (1 - C_{ro}) \left[\frac{T_m - T_c}{1367 - T_c} \right] + C_{ro} \quad (57a)$$

$$C_{ri} = C_{ro} \quad (57b)$$

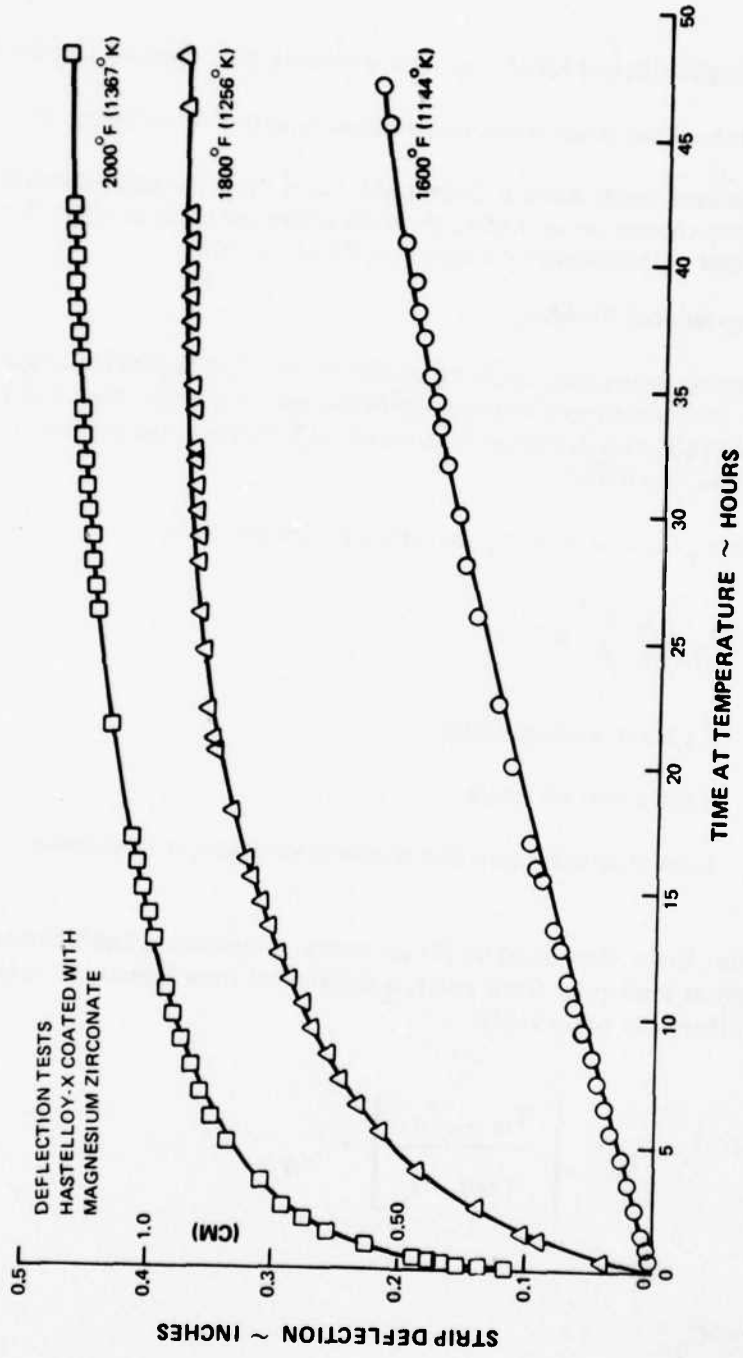


Figure 34 Coating-Induced Buckling Data

where C_{r_0} is the hoop restraint factor for a thermally unbuckled lip (see Figure 35)

T_c is the temperature required to generate a buckling strain ($^{\circ}\text{K}$)

T_m is the lip temperature ($^{\circ}\text{K}$)

For a thermally unbuckled lip, the hoop restraint factor is obtained by treating the lip as a hoop and calculating its resistance to an applied moment. If the lip temperature is 1367°K , it is considered buckled and can be treated as a cantilevered beam. Between the onset of thermal buckling and 1367°K , the hoop restraint is interpolated by Equation 57a.

The strip deflection curves are represented by an equation of the form:

$$\delta = \text{minimum} \quad \left\{ \begin{array}{l} \delta_{\max} \\ \beta t_i^{\rho} \end{array} \right. \quad (58)$$

where β , and δ_{\max} are all functions of temperature (see Figures 36, and 37).

The path dependence of Equations 57 and 58 makes it impossible to incorporate coating-induced buckling into a mission analysis program as stated. When a mix of missions is used to analyze a component life, the life computations must be independent of the sequence in which the missions are flown. In order to make the problem tractable, the model is modified so that the maximum value of C_{r_i} calculated through the mission is used:

$$w_{c_i} = C_{r_{\max}} \left[\frac{L}{1.5} \right]^2 \delta_i \quad (59)$$

In addition, to evaluate the deflection that occurs at any interval in the mission without recourse to a path dependent procedure, the total deflection prior to the interval is used to obtain an equivalent time t^* :

$$\delta_t = \sum_{i=1}^{n-1} \delta_i \quad (60)$$

$$t^* = \left(\frac{\delta_t}{\beta_n} \right)^{1/\rho_n} \quad (61)$$

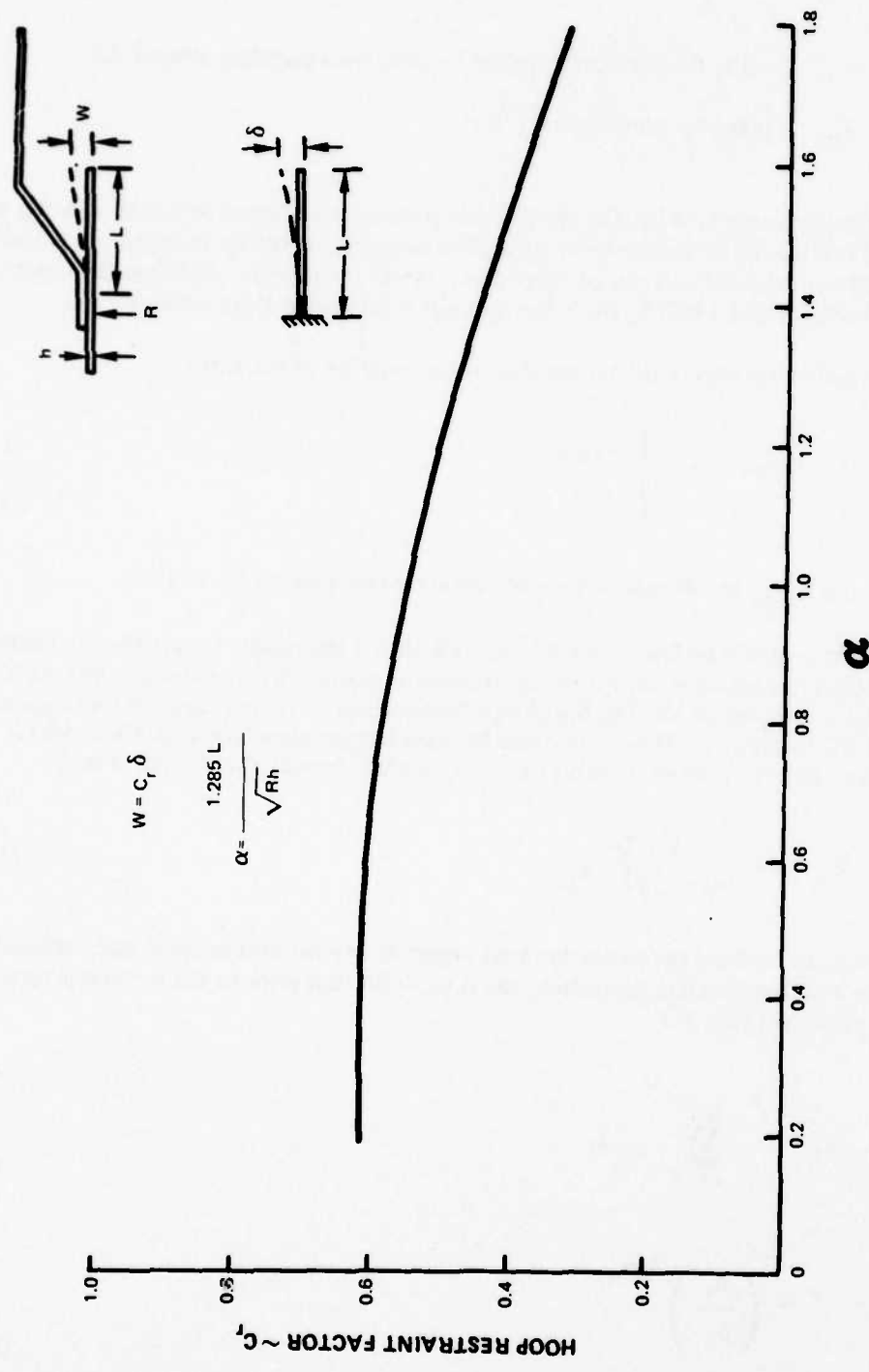


Figure 35 Estimated Hoop Restraint Factor on Axial Bending of Louver Lips Due to Coating Expansion

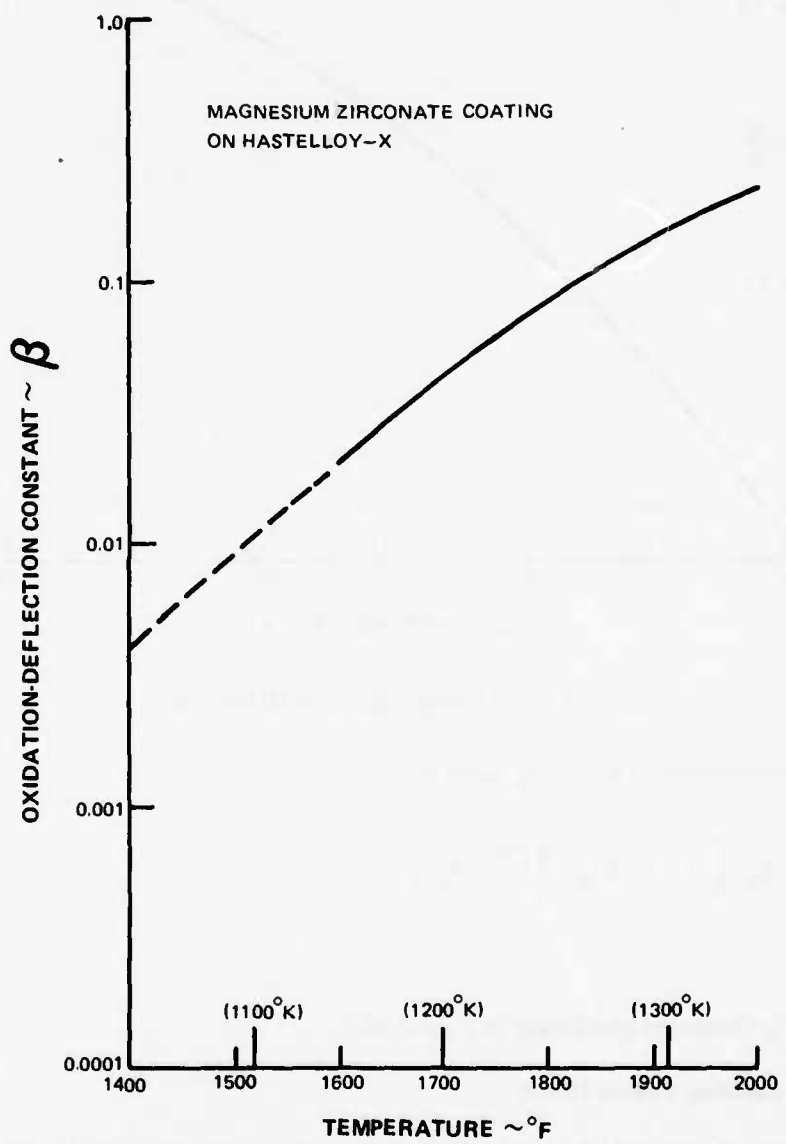


Figure 36 Oxidation-Deflection Constant

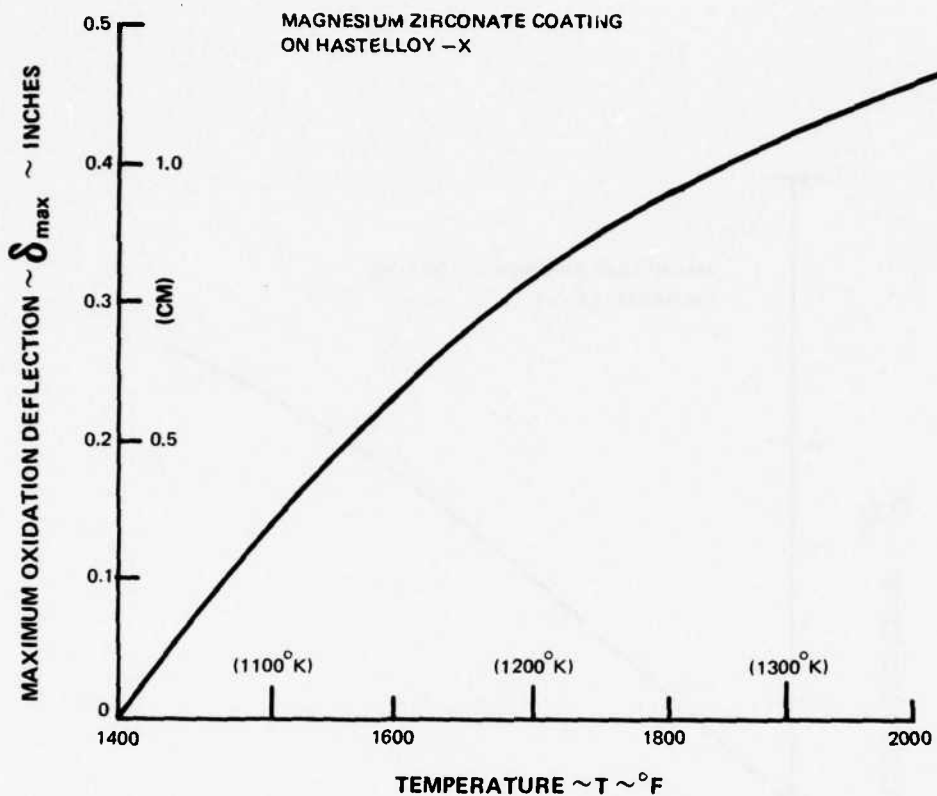


Figure 37 Maximum Oxidation Deflection

The incremental deflection is then computed as:

$$\delta_i = \beta_n \left[t^* + \Delta t_n \right]^{\rho_n} - \delta_{n-1} \quad (62)$$

This procedure is illustrated graphically in Figure 38.

3.2.3.4.3 Lip-Buckling Failure Model

At the conclusion of a mission, the total strip deflection, δ_t , and the total flight time t_t are used to find an equivalent temperature such that the entire mission can be represented by:

$$\delta_t = \beta_t t_t^{\rho_t} \quad (63)$$

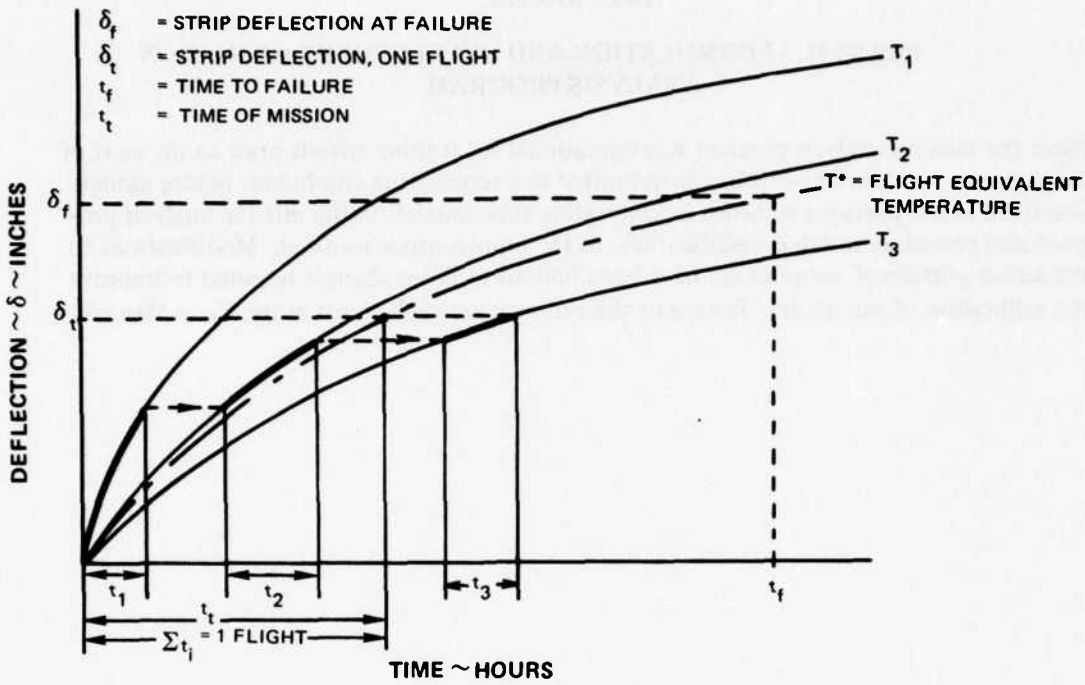


Figure 38 Coating-Induced Buckling Procedure

Since failure is defined as complete lip closure, the strip deflection required for failure is:

$$\delta_f = \frac{W - W_{t\max}}{C_r \max \left(\frac{L}{1.5} \right)^2} \quad (64)$$

and the time to closure is:

$$t_f = \left(\frac{\delta_f}{\beta_t} \right)^{1/\rho_t} \quad (65)$$

The number of cycles to failure is then:

$$N = \frac{t_f}{t_t} \quad (66)$$

SECTION 3.0

PHASE II - FORMULATION AND DEVELOPMENT OF MISSION ANALYSIS PROGRAM

Since the mission analysis program was operational for turbine airfoils prior to the start of the contract, work in Phase II has been limited to encoding the combustor failure models described in the previous sections, incorporating these models in the mission analysis program, and providing suitable modifications to the input/output routines. Modifications to the airfoil portion of the program have been limited to those changes required to improve the calibration of the model. Details of the program are spelled out in the Users Manual.

SECTION 4.0

PHASE III – VERIFICATION OF FAILURE MODELS

4.1 MODEL CALIBRATION

4.1.1 Turbine Failure Model Calibrations

Since the turbine failure models were in existence at P&WA prior to initiation of this contract, work in this area was limited to updating the calibration of the models with recent field service data. Unscheduled engine removal data were used to evaluate the failure models for the JT9D-7. Because the TF30-P-100 engine has not accumulated any unscheduled engine removal (UER) data, scrap mode data was used to calibrate the model.

The calibrations of the JT9D-7 reference models were based on correlations between in-house test data and selected airline statistical plots (Weibull), where at least seven UER data points were used to define each Weibull plot. The reference models are analytical representations of the failure modes of the airfoils.

The JT9D-7 first vane thermal fatigue failure model has been completed. The slope of the fatigue curve (combustor temperature rise $\times \Delta TVR$ vs life in cycles) is set by the results of in-house tests, and its intercept is defined so that the model correlated with field data. ΔTVR is equal to the ratio of the maximum combustor temperature rise to the average combustor temperature rise (maximum turbine inlet temperature - compressor exit temperature)/(average turbine inlet temperature - compressor exit temperature).

The JT9D-7 first blade creep/fatigue model correlated with the statistical data. Therefore, no further work was required.

The JT9D-7 first blade oxidation/corrosion model defining coating depletion and base metal attack was based upon in-house testing. The model was then calibrated empirically to match the statistical data. This approach is required because of the difficulty in determining, by in-house testing, when an airline operator defines the airfoil as being a UER.

The JT9D-7 second-vane calibration was directed at defining the characteristic gas temperature of the vane (i.e., the gas temperature at the first vane to fail). Using the calculated vane cooling effectiveness, average gas temperature, and combustor pattern factor, the characteristic gas temperature that would match mission analysis predictions with airline experience was determined.

The JT9D-7 second-blade reference model was calibrated using data for a heavy-tip blade which is currently being removed from service. Since there is little experience with the light-tip replacement, an empirical correction factor is employed to convert the model from the heavy-to the light-tip blade. This adjustment has been calibrated by in-house testing and the limited field data available.

For the TF30 P-100, reference models were developed using in-house endurance data. Reference models were developed for first-blade creep, second-blade creep, second-blade under-shroud cracking, second-vane oxidation/corrosion, and third-blade creep/failure modes.

4.1.2 Combustor Failure Model Calibrations

4.1.2.1 Creep-LCF Model

The condition of a number of JT9D-7 combustors at engine removal was noted in detail in a special airline survey conducted at P&WA. A representative sampling of airlines was used including a range of "tough" - full-rating, hot-climate - to "easy" - de-rated, cold-climate - operators. Data was obtained for combustors with up to 8000 hours of operation. The combustor was not necessarily the cause of engine removal.

Figure 39 shows the data taken from the damage surveys. The plotted symbols indicate the results of the inspections (cycles) plotted at the estimated maximum metal temperature for the particular louver and flight condition. The temperature estimates were derived from analysis, confirmed by thermocouple measurements in experimental engines. The open symbols indicate that no cracking distress was observed at inspection while shaded symbols indicate louvers in which cracking was observed. The critical regions in this combustion chamber are found to be in the front end of the outer liner and in the aft end of the inner liner.

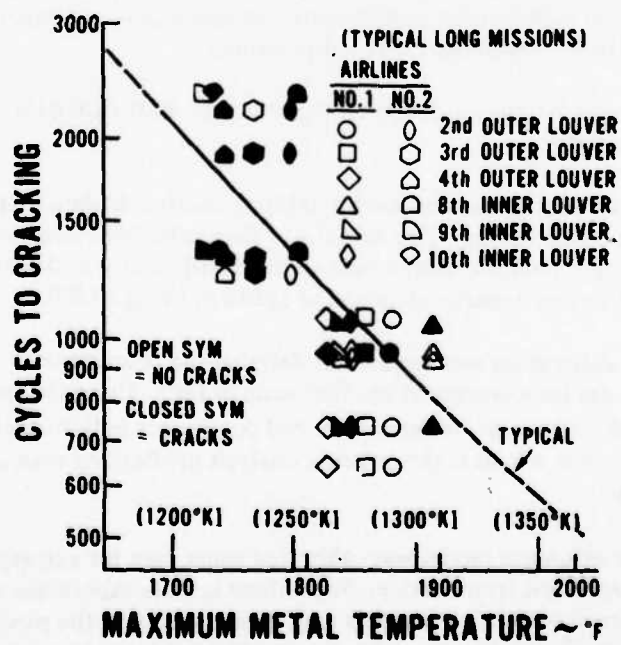


Figure 39 JT9D-7 Combustor ~ Comparison of Mission Life Predicted by Creep - LCF Failure Model with Field Service Data

The curve drawn in Figure 39 represents the typical mission life predicted by the creep/LCF failure model. Mission life is calculated from the linear accumulation of damage at the sea-level takeoff, climb, cruise, and thrust-reverse operating points.

Application of the failure model to a typical can-annular combustor configuration is demonstrated in Figure 40. The data is taken from a rig test of a section of a combustor in which the louver lip is alternately heated and cooled between 1600°F (1144°K) and room temperature. Also shown in this figure is the observed life in the mode of failure of the particular configuration tested in airline service and the data of Figure 40 for the JT9D-7. The data is plotted as predicted life versus observed life (cycles). Almost all of the predictions fall within a factor of two of the observed lives. Considering the uncertainty involved in the observed data and the predicted metal temperature, and the accuracy claimed for the strain range partitioning method, the results were considered very encouraging.

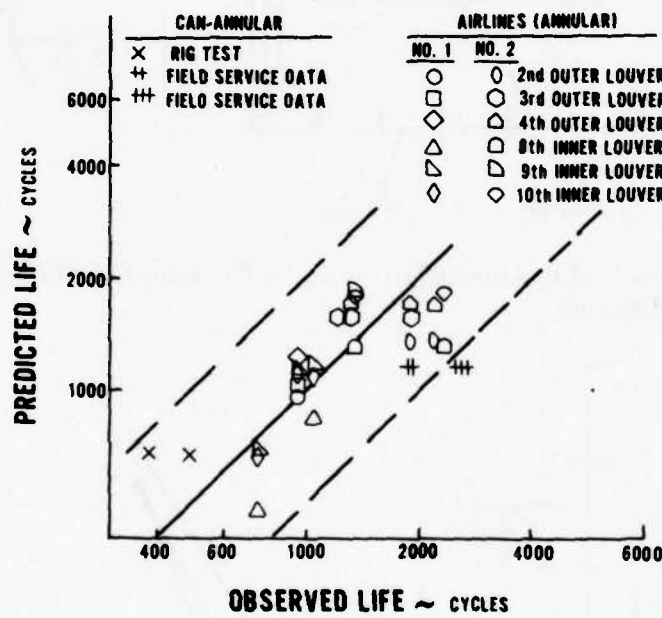


Figure 40 Comparison of Creep-LCF Life Prediction with Field Service Experience

4.1.2.2 Louver-Lip Buckling Model

Calibration of the thermal buckling portion of the louver-lip buckling model was accomplished by rig testing. As part of an in-house test program conducted at P&WA, louver-lip buckling data was obtained in a fluidized bed test. A schematic of the test rig is shown in Figure 41. The test specimen was held in the fluidized bed with the lip and seam weld heated while cooling air reduced the temperature of the cold knuckle portion, thereby imposing a gradient upon the structure. The test specimen was run with the hot portion at 1700°F (1200°K) and progressively higher gradients were imposed until the onset of buckling was observed. The louver-lip buckling model predicted that at 1700°F (1200°K) a gradient of 675°F (375°K) would be required to buckle the test specimen louver. Figure 42 is a plot of

measured deflection vs lip-to-knuckle gradient for the test specimen. The sharp change in slope indicates that buckling occurs at a gradient of between 660 and 675°F (367 and 375°K) indicating excellent agreement between prediction and data.

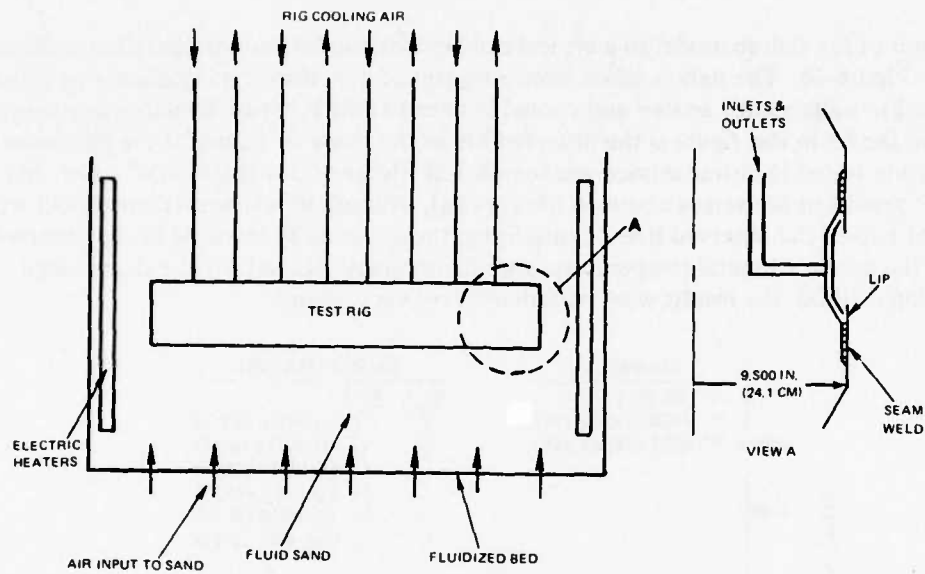


Figure 41 Schematic of Fluidized Bed Test Rig for Obtaining Combustor Louver Lip Buckling Data

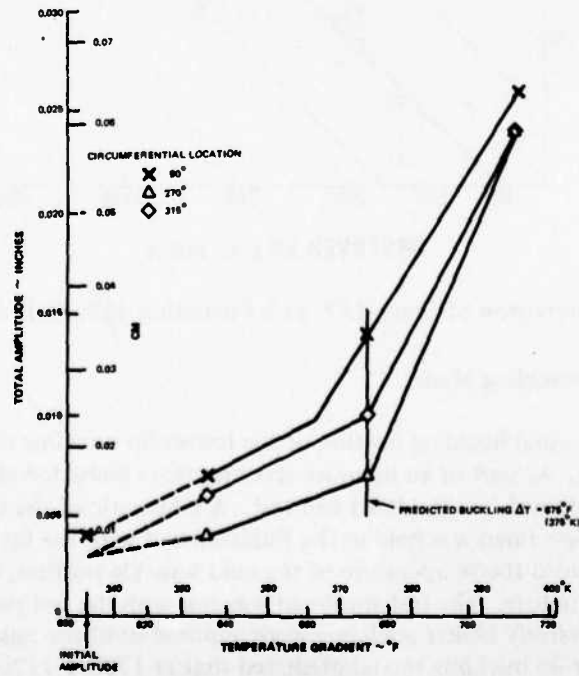


Figure 42 Calibration of Louver Lip Thermal Buckling Model

4.1.2.3 Verification With JT9D-70 Burner Data

At the time the burner failure models were being developed, the JT9D-70A was just beginning to undergo in-house endurance testing and field service evaluation. The burner models were used to predict the life of the liners as a function of temperature.

For the relatively long flight time case (4 hours), depicted for the outer liner in Figure 43, the predominant failure mechanism is expected to be louver lip collapse. The problem here is basically time at temperature rather than cycles. An early inspection of a service liner indicated that lip collapse would be the failure mode, confirming the model. There was no indication of cracking.

In the shorter flight time case (1.6 hours), illustrated in Figure 44 for the inner liner, the relative importance of the creep-LCF life has increased to the point that cracking would be the primary failure mode. Here again, preliminary examination of the service hardware confirmed the prediction. Cracking had begun to occur while there was no sign of lip buckling.

Figures 43 and 44 confirm the validity of the two combustor failure models. In the long flight time case, the program predicts and experience confirms that lip buckling will be the primary failure mode. In the short flight time case, cracking is predicted to be the primary failure mode, and again, this is confirmed by observations.

4.2 UNCERTAINTY ANALYSIS

The purpose of this portion of the contract was to determine the sensitivity of the lives predicted by the model to variations in the input parameters. The usefulness of the model is doubtful if a change in an input parameter of a magnitude consistent with its uncertainty, produces a large change in the predicted life.

4.2.1 Turbine Airfoils

Table 3 lists the variables to be perturbed to evaluate the sensitivity of the turbine airfoil models. The results of the uncertainty analysis for the airfoils are summarized in Table 4. In each engine (TF30 and JT9D) a typical mission and conditions were selected to produce a reference B-50 life based upon the following conditions:

- (1) Minimum material properties.
- (2) Average values of compressor, combustor and high turbine inlet temperatures.
- (3) An average combustor exit radial profile consistent with a half-deteriorated engine.

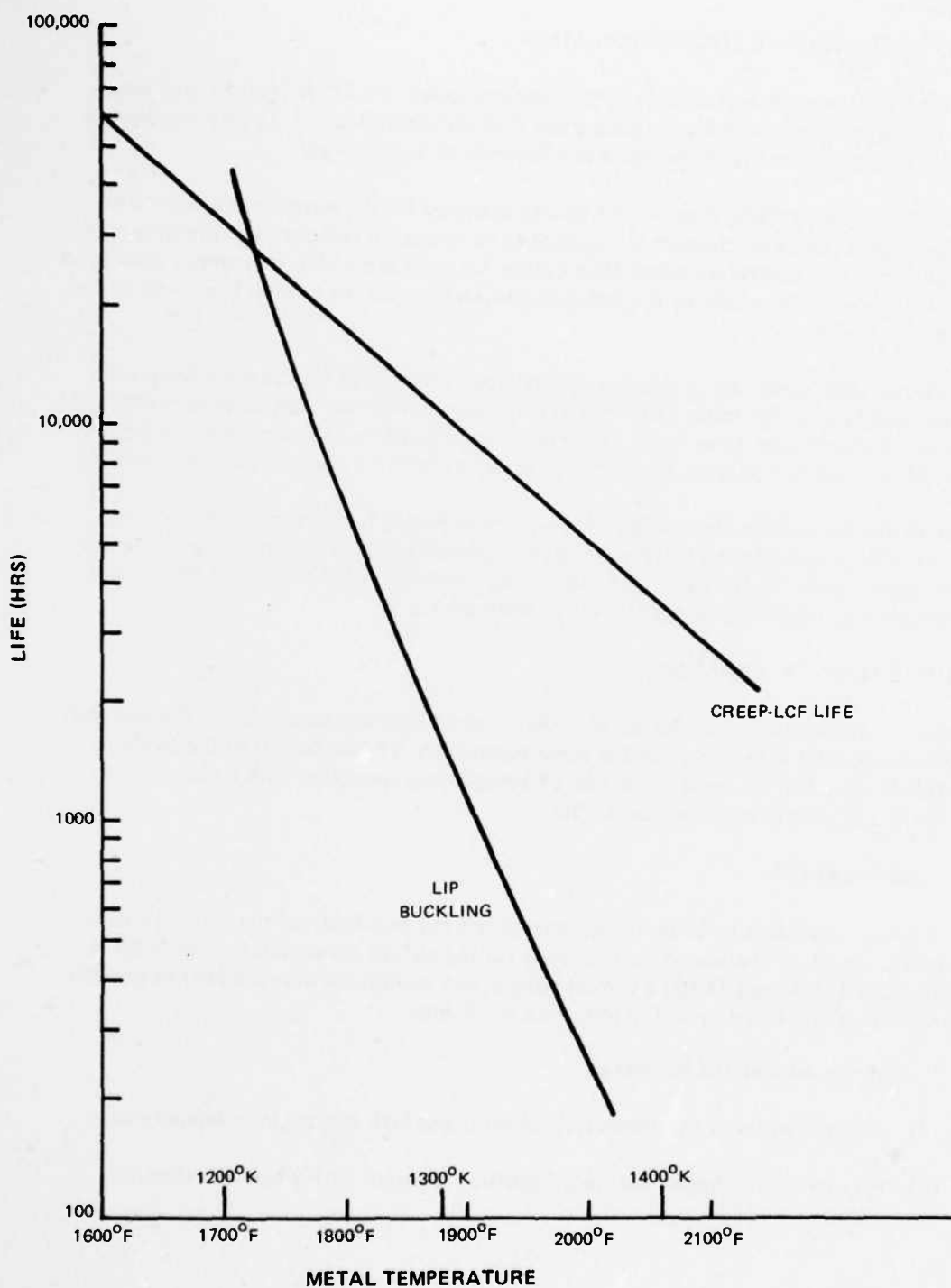


Figure 43 Design Application of Burner Failure Models – JT9D-70 Outer Liner
(4-Hour Flight)

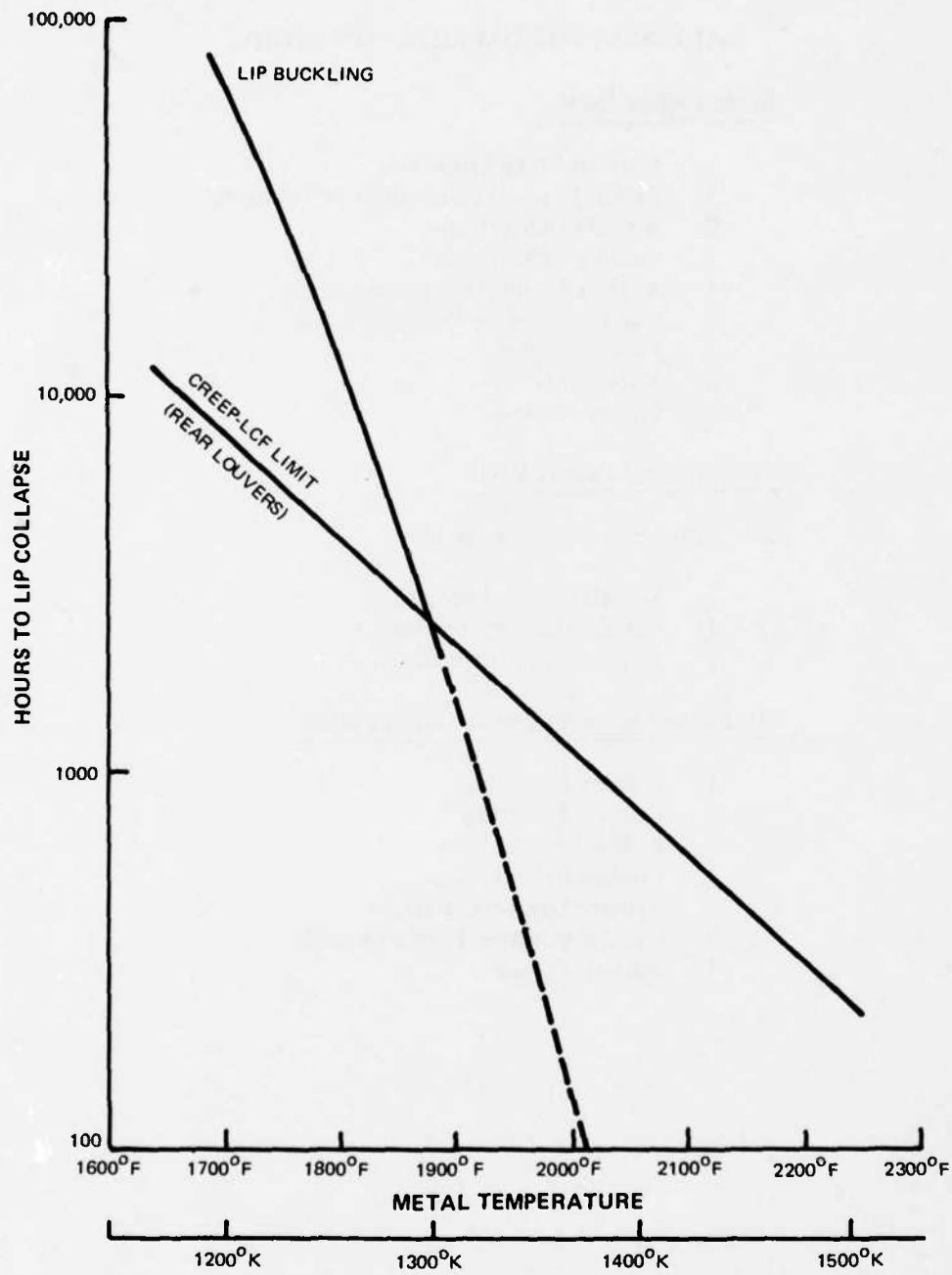


Figure 44 Design Application of Burner Failure Models – JT9D-70A Inner Liner (1.6-Hour Flight)

TABLE 3
VARIABLES FOR UNCERTAINTY STUDY

Creep Failure Mode

1. Material Creep Properties
2. Airfoil Physical Dimensions (Tolerances)
3. Airfoil Cooling Flow
4. Cooling Effectiveness
5. Average Engine Gas Temperatures
6. Gas Temperature Profile (Radial)
7. Pattern Factor
8. Rotor RPM
9. Engine Airflow

Creep-Fatigue Failure Mode

Same as those for creep, plus:

10. Material Fatigue Properties
11. Engine Transient Operation
12. $T_{\text{gas}} - T_{\text{cool}}$ Differences

Oxidation/Corrosion/Erosion Failure Modes

1. Coating Properties
2. Coating Thickness
3. Airfoil Cooling Flow
4. Cooling Effectiveness
5. Average Gas Temperatures
6. Gas Temperature Profile (Radial)
7. Pattern Factor

TABLE 4 - TURBINE UNCERTAINTY ANALYSIS

ENGINE REFERENCE LIFE (HR)	JT9D-7						TF30-P100					
	1st Vane	1st Blade	2nd Vane	2nd Blade	1st Blade	2nd Vane	1st Blade	2nd Vane	1st Blade	2nd Vane	Undershroud	2nd Blade
Airfoil												Creep
Failure Mode	Fatigue	CRP-FAT	CRP-FAT	CRP-FAT	CRP-FAT	CRP-FAT	CRP-FAT	CRP-FAT	CRP-FAT	CRP-FAT	Cracking	Creep
Uncertainty Variations												
Mat Creep Prop. + 1.0%	*	1.01	*	1.01	1.01	*	*	1.01	*	1.01	1.01	1.01
Mat Creep Prop. -1.0%	*	0.99	*	0.99	0.99	*	*	0.99	*	0.99	0.99	0.99
Avg. T_{GAS} + 20°F	0.93	0.86	0.88	0.85	0.76	0.82	0.86	0.74	0.77	0.77	0.72	
Avg. T_{GAS} -20°F	1.08	1.18	1.16	1.20	1.48	1.28	1.20	1.55	1.44	1.44	1.54	
ΔTVR + 0.02	0.93	*	*	*	*	*	*	*	*	*	*	*
ΔTVR - 0.02	1.08	*	*	*	*	*	*	*	*	*	*	*
RPM + 80/150***	*	0.94	*	*	0.90	0.91	*	0.86	0.86	0.86	0.86	
RPM - 80/150***	*	1.06	*	*	1.12	1.11	*	1.20	1.20	1.20	1.18	
Cooling Effectiveness + 1.0%	**	0.92	0.92	0.91	0.94	0.86	0.92	0.91	0.90	0.90	*	
Cooling Effectiveness - 1.0%	**	1.09	1.10	1.11	1.07	1.18	1.09	1.11	1.12	1.12	*	
Radial T_{GAS} Profile Shift	**	1.08	*	0.87	0.98	1.06	*	0.74	1.10	1.09		
Airfoil Cooling Airflow - 10%	**	0.78	0.88	0.76	0.85	0.69	0.95	0.93	0.80	*		
Airfoil Cooling Airflow + 10%	**	1.38	1.17	1.44	1.11	1.92	1.06	1.08	1.30	*		
Transient Operation + 1.0%	**	0.98	*	0.99	*	*	*	*	*	*	*	
Transient Operation - 1.0%	**	1.02	*	1.01	*	*	*	*	*	*	*	
Fatigue Prop. + 1.0%	**	1.03	*	1.03	*	*	*	*	*	*	*	
Fatigue Prop - 1.0%	**	0.97	*	0.97	*	*	*	*	*	*	*	

*Does not apply.

**Not possible to separate from model.

***80 RPM for JT9D/150 RPM for TF-30.

For each perturbation, the baseline conditions were utilized, as noted in the column under uncertain variations.

The results are reported as life divided by base life for an incremental change in the baseline condition. As an example, the creep-fatigue life of the JT9D-7 first blade would be 1.01 (0.99) times the base life for a 1% increase (decrease) in material creep properties. Asterisks appear for those items for which uncertainty in the parameter will have no effect on the part or failure mode. For example, transient operation is the rate at which the engine conditions are shifted. This in turn affects thermal gradients and is reflected only in the life of parts with fatigue failure modes. The other columns have asterisks.

The failure model for the first vane differs from the models for other components. It involves a relationship between gas temperature and life. The relationship is determined for one operating condition by a two-dimensional thermal analysis and a stress analysis and is then calibrated with test engine data. The lack of field data is the reason there are no values in Table 4 for the TF30 first vane. Crack propagation rate data is then used to extend the analysis at one point to a general model. Parameters such as material properties and film effectiveness do effect the life of the first vane but they cannot be perturbed in the model. They are built into the analysis at the reference condition.

One exception to the procedure of perturbing a parameter above and below a baseline value is the burner exit radial profile. An arbitrary shift (see Figure 45) in the combustor exit radial profile has been imposed to determine its effect on airfoil life.

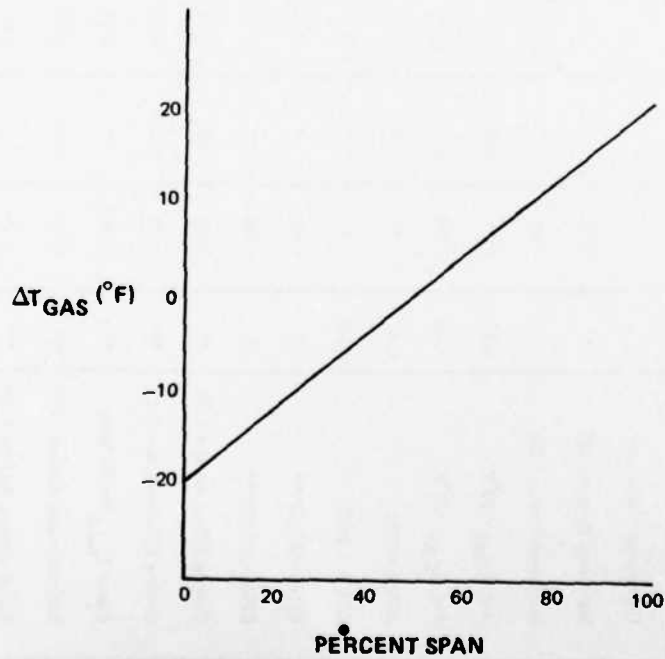


Figure 45 Radial Gas Profile Shift

4.2.2 Burner Analysis

The results of the corresponding analysis for burners is presented in Table 5 for the creep-low cycle fatigue (cracking) failure model and in Table 6 for the louver lip buckling model. The base life calculation was performed for an annular, film cooled burner of louvered, sheet metal construction (JT9D) on a typical commercial mission. The symbols along with the variable description are consistent with the nomenclature used in Section 2.2.

Some care should be exercised in interpreting the results of the lip buckling uncertainty analysis. The lip buckling involves two phenomena: thermal and coating-induced buckling. Thermal buckling may or may not occur for any given situation, while the coating-induced buckling always occurs at a rate that is a function of time and temperature. Therefore, the results of any uncertainty analysis will strongly depend on the base case selected.

The relative insensitivity of lip buckling to the various material moduli is partially a result of the two-phenomena mechanism described above and partially a result of the manner in which the moduli enter the calculations. For example, equation 53 is used to calculate the equivalent elastic stress required for lip buckling. The modulus terms appear in both numerator and denominator, roughly canceling the effect of the perturbation.

The large increase in louver lip buckling life that occurs when the metal temperature is dropped 100°F is also due to the two-phenomena mechanism of the model. With the metal temperature reduced 100°F (55.6°K) the lip did not exceed the critical buckling temperature and closure of the lip is due only to the coating volume change.

TABLE 5
PHASE III BURNER CRACKING MODEL UNCERTAINTY ANALYSIS
Reference Life = 4400 Hrs.

Variable	Variation	Life/Base Life
Youngs Modulus (E)	+10%	1.04
	-10%	0.95
Plastic stress-strain relationship (K_1)	+50%	1.12
	-50%	0.83
Tensile ductility (D_p)	+50%	1.84
	-50%	0.61
Endurance limit strain range	+25%	1.17
	-25%	0.88
Time dependent plastic stress-strain relationship (B_t)	+50%	0.96
	-50%	1.09
Hoop strain thermal gradient proportionality (C_H)	+25%	0.75
	-25%	1.65
Time at take-off	+25%	0.96
	-25%	1.02
Metal temperature	+100°F	0.66
	-100°F	1.86

TABLE 6
PHASE III BURNER LOUVER LIP BUCKLING UNCERTAINTY ANALYSIS

Reference Life = 3200 Hrs.

Variable	Variation	Life/Base Life
Young Modulus (E)	+10%	0.99
	-10%	1.02
Secant/Tangent Modulus (Es/Et)	+10%	1.02
	-10%	0.98
Coating Expansion Modulus (β)	+25%	0.68
	-25%	1.65
Buckling Amplitude (W_t)	+25%	0.84
	-25%	1.16
Metal Temperature	+100°F	0.21
	-100°F	11.76
Lip Length (L)	+0.05 in.	0.71
	+0.15 in.	0.58
Lip Thickness (h)	-0.005	0.93
	+0.005	1.10

SECTION 5.0

PHASE IV – MISSION MIX LIFE SENSITIVITY STUDY

5.1 MISSION ANALYSIS LIFE PREDICTION

The calibrated mission analysis-life prediction computer program was used to predict the B-50 life of each of the modified components for a baseline mission and three alternate missions. The turbine airfoils were evaluated in both a transport (JT9D-7) and a fighter/attack (TF30-P-100) propulsion system, using suitable missions for each powerplant. Since the only data available to calibrate the combustor failure models during the period of the contract came from the commercial JT9D-7, only a transport mission mix was applied to the combustor. For similar reasons, meaningful lives could not be generated for the JT9D engine at fighter/attack aircraft operating conditions.

5.1.1 Transport Mission

The baseline transport mission was a typical four-hour full-rated commercial mission consisting of take off, climb to dispatch altitude, cruise to destination and landing. The three alternate missions were full rated two- and six-hour missions and a four-hour derated mission with derated takeoff and climb. The common characteristics of the four flights were:

Take Off Gross Wt	600,000 lbs (272,000 kg)
Dispatch Altitude	33,000 ft. (10,000 m)
Take Off Ambient Temperature	64.6°F (18.1°C)
Cruise Mach No.	0.84
Climb Characteristic	250/340/.81

The climb characteristic describes the climb as 250 knots up to 10,000 ft. (3000 m) and then 340 knots until a speed equal to .81 Mach number is reached. In the derated mission, the angle of attack is lower and the aircraft takes longer to reach dispatch altitude. Because of the lower power requirements the component operating temperatures are lower.

The component life predictions are summarized in Table 7. The benefits in durability of flying derated becomes apparent when the two four-hour missions are compared. The manner in which life, in hours, increases with the duration of the mission underscores the importance of the number of cycles on component lives. Much of the hot-section damage to components occurs at take-off and climb and an aircraft flying only two-hour missions takes off 3 times as often as one flying six-hour missions for the same total flight time.

TABLE 7
HOT SECTION COMPONENT LIFE PREDICTIONS (B-50 UER)
FOR TRANSPORT (JT9D) MISSIONS IN HOURS

Airfoil	1st Vane	1st Blade	1st Blade	2nd Vane	2nd Blade	Combustor	
Mission \ Failure Mode	Fatigue	Creep Fatigue	Oxidation Corrosion	Creep Fatigue	Creep	Creep-LCF	Lip Buckling
Derated 4 hr. Mission	14400	6900	7300	10400	16500	5600	4000
Full Rated 2 hr. Mission	5600	1900	3600	2100	3200	2100	1800
Full Rated 4 hr. Mission	11700	3900	6100	4300	6600	4400	3200
Full Rated 6 hr. Mission	17800	6000	8100	6600	10100	6700	4300

5.1.2 Fighter/Attack Mission

The four TF30-P-100 missions selected from the F-111 aircraft were a functional check flight profile mission, a training mission (baseline), a transition profile mission and a radar score profile mission. A detailed description of these missions can be found in the Appendix. The last three missions were run without any touch and go landings. The predicted lives for the missions are summarized in Table 8.

TABLE 8
TURBINE COMPONENT LIFE PREDICTIONS (B-50 SCRAP)
FOR FIGHTER/ATTACK (TF30-P-100) MISSIONS IN HOURS

Airfoil	1st Blade	2nd Vane	2nd Blade	2nd Blade	3rd Blade
Mission \ Failure Mode	Creep	Oxidation/Corrosion	Undershroud Cracking	Creep	Creep
Functional Check Flight Profile	1700	1600	700	6000	1700
Training Without Touch and Go	2800	2400	1000	8300	2800
Transition Profile Without Touch and Go	2800	2000	900	7700	2500
Radar Score Profile Without Touch and Go	9300	7000	3200	27000	8900

5.1.3 Mission Mix Sensitivity

A study was performed to establish the sensitivity of the failure models to perturbations in mission parameters. Tables 9 and 10 present the results of the study for the JT9D-7 and TF30-P-100 respectively. In Table 9 the results shown in Table 7 for the four-hour, full rated mission, selected as the baseline, have been repeated at the top of the table, and the results of the various perturbations have been reported as life divided by base life. Similarly, Table 10 presents the results of the study for the TF30-P-100 with the training mission selected as a baseline. The perturbations associated with take-off gross weight and climb for the TF30-P-100 were not included because aircraft rated performance information (as opposed to engine performance) was not available.

TABLE 9

MISSION PARAMETER SENSITIVITY STUDY, JT9D-7 HOT SECTION COMPONENTS

Airfoil	1st Vane	1st Blade	1st Blade	2nd Vane	2nd Blade	Combustor	
Failure Mode	Fatigue	Creep/ Fatigue	Oxidation Corrosion	Creep- Fatigue	Creep	Creep- LCF	Lip Buckling
Mission Parameter	Life/Base Life						
Baseline 4 hr. full rated mission	11700	3900	6100	4300	6600	4400	3200
Ambient temperature +5 C	0.94	0.76	0.76	0.79	0.71	0.88	0.74
Ambient Temperature -5 C	1.08	1.55	1.48	1.48	1.87	1.16	1.61
Take off Gross Weight + 10,000 lbs.*	1.0	0.92	0.96	0.96	0.99	1.0	0.96
Take off gross weight - 10,000 lbs.*	1.0	1.01	1.04	1.00	1.01	1.0	1.04
Dispatch altitude +1000 ft**	1.0	0.99	0.96	1.0	1.0	1.0	1.01
Dispatch altitude - 1000 ft.**	1.0	1.0	1.0	1.0	1.0	1.0	0.98
Cruise Mach Number +.01	1.0	1.0	0.96	1.0	1.0	1.0	0.96
Cruise Mach Number -.01	1.0	1.0	1.03	1.0	1.0	1.0	1.04
Climb airspeed +5 knots	1.0	0.98	0.99	0.99	0.98	1.0	0.98
Climb Airspeed -5 knots	1.0	1.02	1.01	1.01	1.02	1.00	1.02
Climb Mach Number +.01	1.0	1.0	0.99	1.0	0.99	1.0	0.99
Climb Mach Number -.01	1.0	1.01	1.01	1.01	1.01	1.0	1.01
Block Time +15 minutes	1.06	1.06	1.04	1.06	1.06	1.06	1.05
Block Time - 15 minutes	0.94	0.94	0.96	0.94	0.94	0.94	0.95

* 4350 kg

** 305m

TABLE 10
MISSION PARAMETER SENSITIVITY STUDY, TF30-P-100 TURBINE COMPONENTS

Airfoil	1st Blade	2nd Vane	2nd Blade	2nd Blade	3rd Blade
Failure Mode	Creep	Oxidation/ Corrosion	Undershroud Cracking	Creep	Creep
Mission Parameter	Life/Base Life				
Baseline Training Profile Mission	2800 hrs.	2400	1000	8300	2800
Ambient Temperature +5 C	0.82	0.88	0.84	0.84	0.84
Ambient Temperature -5 C	1.35	1.20	1.32	1.32	1.32
Dispatch Altitude +1000 ft. (305m)	1.10	1.06	1.09	1.10	1.09
Dispatch Altitude - 1000 ft. (305m)	0.94	0.96	0.94	0.94	0.94
Cruise Mach Number +.01	0.97	0.98	0.97	0.97	0.97
Cruise Mach No. -.01	1.04	1.02	1.04	1.04	1.04
Block Time +15 minutes	1.10	1.10	1.10	1.10	1.10
Block Time -15 minutes	0.90	0.90	0.90	0.90	0.90

The greater sensitivity of the fighter/attack aircraft to dispatch altitude relative to the transport is related to the type of mission. The transport climbs to a dispatch altitude once, and then cruises while the fighter/attack aircraft climbs to altitude several times within a mission and the 1000 ft (305 m) increment is applied each time.

REFERENCES

1. "Reliability Prediction for Combustors and Turbines", Interim Technical Report, PWA-5350, Dec. 1975.
2. J. F. Polhemus, C. E. Spaeth and W. H. Vogel, "Ductility Exhaustion Model for Prediction of Thermal Fatigue and Creep Interaction", Fatigue at Elevated Temperatures, ASTM STP 520, American Society for Testing and Materials (1973) pp. 625-635.
3. S. S. Manson, "The Challenge to Unify Treatment of High Temperature Fatigue - A Partisan Proposal Based on Strainrange Partitioning", Fatigue at Elevated Temperatures, ASTM STP 520, American Society for Testing and Materials (1973) pp. 744-782.
4. B.F. Langer, "Design of Pressure Vessels for Low-Cycle Fatigue," Journal of Basic Engineering, Trans. ASME, Series D, Vol. 84 (1962) p. 389.
5. J. Marin, "Mechanical Behavior of Engineering Materials," Prentice-Hall, Inc. Englewood Cliffs, N. J. (1962).
6. F. R. Larson and J. Miller, "A Time-Temperature Relationship for Rupture and Creep Stresses", Trans. ASME Vol. 74 No. 5 (1952) p. 765.
7. S. S. Manson and A. M. Halford, "A Linear Time-Temperature Relation for the Extrapolation of Creep and Stress-Rupture Data," NACA Tech. Note 2890.
8. A. Mendelson, M. H. Hershberg and S. S. Manson, "A General Approach to the Practical Solution of Creep Problems," J. Basic Engineering, Dec. 1959, pp. 585-598.

APPENDIX

TABLE A-1
FUNCTIONAL CHECK FLIGHT PROFILE

Power Setting (N2)	Time	Alt (1,000 ft.)	Mach No.
1. Idle	50 min	Ground level	a. 2 Cycles 75% N2 back to idle. b. 1 min at Mil back to idle. c. 1 min at Max A/B back to idle. d. 15 sec at Mil back to idle
2. Max AB	3 min	15	.65 Takeoff & climb
3. Idle	1 min	15	.45 Decelerate
4. 85%	1 min	15	.45 Angle of attack & airspeed check
5. Mil	1 min	15	.70 Accelerate
6. 85%	5 min	15	.75 Climb
7. Mil	2 min	20	.75 Level off
8. 90%	1 min	20	.75 Level off
9. Idle	2 min	20	.35 Gear cycle decelerate
10. Mil	2 min	20	.75 Accelerate
11. 85%	8 min	20	.75 Cruise
12. Mil	3 min	30	.75 Climb
13. 90%	1 min	30	.75 Level off
14. Min A/B (Zone 1)	1 min	30	.9 Min A/B stop check
15. Mil	5 min	30	.9 Stabilize
16. Max A/B	1 min	30	1.1 Accelerate
17. Max A/B	2 min	40	1.1-1.4 Climb
18. Max A/B	2 min	41	2.2 Accelerate
19. Max A/B	2 min	50	2.2 Climb
20. Min A/B	1 min	50	1.5 Decelerate
21. Mil	1 min	30	1.5-.9 Descent decelerate
22. 80%	2 min	15	.85 Descent
23. Idle	1 min	4	.78 Descent to TFR
24. 88%	15 min	4	.78 TFR
	a. 25 cycles \pm 4% N2		
	b. 4 cycles up to Mil for 30 sec duration.		
	c. 4 cycles from Mil to 80% for 30 sec duration.		
25. Mil	2 min	11	.78 Climb
26. Idle	2 min	11	.4 Decelerating
27. 90%	2 min	11	.4 Gear warning check
28. Mil	2 min	11	.75 Accelerating
29. 80%	10 min	4	.32 Landing pattern
30. 90%	5 min	4 Ground level	Landing
31. Idle	20 min	Ground Level	Taxi
	One cycle up to 75% after landing		

TABLE A-2
TRAINING PROFILE

Power Setting (N2%)	Time	Alt (1,000 ft.)	Mach No.
1. Idle (68%)	50 min	Ground level	.0 Gnd start up Alignment of IRS and taxi
2. Max AB	1 min	1	.65 Takeoff
3. Military	8 min	20 (18-22 MSL)	.75 Climb
4. 85%	20 min (Avg Time)	20	.73 Cruise
5. 80%	3 min	7 (Avg Alt)	.8 Letdown
6. 88%*	55 min*** (30 min TFR)	0.5-1.0 TFR 500 to **** 1000' AGL	.75
7. Military	6 min	20	.75 Climb
8. 83%	15 min	20	.73 Cruise
9a. 90% to Max AB	15 min	15-20	.88 Defensive Combat
9b. 85 to Mil	20 min	10-22	.85 Maneuvering
10. Idle (68%)	3 min	4	.5 Descent
11. 80%	10 min	4	.32 Approach
12. 90%	5 min	4-1	.3 Turn to final, final approach
13. Idle to Mil**	15 min	1-3	.3 Touch & goes
14. Idle (68%)	20 min	Ground level	.0

* 100 throttle excursions of at least $\pm 4\%$ from stabilized RPM.

** 3-5 throttle excursions (3 touch & go landings on about 15% of all training missions).

*** 30 min TFR penetration to bomb drop. ~25 min circular pattern for additional bomb drops.

Subsequent to a bomb drop a full Mil power 1 min climb to 3000', reduce power for down-wind leg 180° from drop path (2 min), descent (70-75% power), 180° descending turn to bomb run.

****50% at 500', 50% at 1000'

TABLE A-3
TRANSITION PROFILE

Power Setting (N2)	Time	Alt (1000 ft)	Mach No.
Items 1, 2 same as training profile.			
3. MIL	6 MIN	13	.75 Climb
4. 85%	45 MIN	13	.73 Cruise
5. 90%*	35 MIN		Airwork
6. Same as Items 10-14 of the training profile with 3 touch and go landings on 100% of these flights			Penetration

*Doing Lazy 8's, Wing Sweeps, Penetrations, Max Power Climbs, many throttle movements between idle to zone 5.

- (5) Lazy 8 - 80% - MIL - 3 min each
- (4) Chadel - Military - 1.5 min each
- (1) Max Power Climb to 30-35K ' - 3 min
- (2) Simulated Traffic Pattern at Alt - 5 min similar to steps 6, 7, 8 of Instruments Profile

TABLE A-4
RADAR BOMB SCORE (RBS) PROFILE

Power Setting (N2)	Time	Alt (1000 ft)	Mach No.
Items 1, 2, 3 same as training profile			
4. 85%	30 min	20	.73 Cruise
5. 85%	10 min	12	.74 Letdown
7. 87%	40 min	10	.75 Straight & Level
8. MIL	3 min	15	.75 Constant Speed Climb
9. 83%	10 min	15	.75 Bomb Run Straight & Level
10. 80%	30 min	15	.73 Big Circle To Re-enter Bomb Run
11. 83%	10 min	15	.75 Straight & Level Bomb Run
12. 80%	15 min	15	.73 Return To Base

Items 10, 11, 12, 13 and 14 from training profile including three touch and go landings on 15% of flights.

